Verification Analyses for Computer Program

B.1 Introduction

To check the results obtained from the transient thermal hydraulic computer program, several test problems which have analytic solutions or allow comparison to experimental data were run using the program. These test problems were chosen to check those features of the program which were considered important for the _____ auxiliary feed pump turbine piping analysis. Important parameters for this analysis were considered to be as follows:

1. The conduction of heat to the pipe wall from the fluid which is responsible for the condensation of steam.

2. The heat transfer coefficient between the pipe wall and the fluid. This coefficient includes regions of free convection, forced convection, and condensation heat transfer.

3. The slip model which determines the rate at which separation of water and steam occur in the piping. The time at which the water accumulates

B.2

at the inlet to the turbines is dependent on this model although the total water available would probably not be very sensitive to this parameter.

4. The conservation of mass, momentum, and energy as solved by the program including the appropriate equations of state.

B.2 Comparison to Analytic Solution of Heat Conduction Through a Cylindrical Wall

Figure B1 shows the computer model which was used to obtain the solution for the transient conduction heat transfer through a cylindrical wall similar to that which exists in the _   _ auxiliary feed pump turbine piping. The pipe wall was assumed to be at an initial uniform temperature of 100 degrees Fahrenheit and a constant heat transfer coefficient of 0.2 Btu/sec/sq ft/deg F was assumed for the inside surface of the wall with the fluid temperature at 500 degrees Fahrenheit. The outside wall of the pipe was considered perfectly insulated. The solution obtained using the thermal hydraulic computer program, assuming several different numbers of elements through the pipe wall, is compared to an analytic solution for this problem in Figure B2. The comparison indicates that the thermal hydraulic computer program provides

B.3

reasonable answers to this problem and that the pipe
wall can be adequately modeled by four elements across
its thickness.

B.3   Reasonableness of Heat Transfer Coefficients
The thermal hydraulic computer program used for this
analysis provides as part of the print-out the
equivalent heat transfer coefficient for each heat flow
path. The magnitude of the heat transfer coefficients
were checked for reasonableness against hand
calculations and published results.

B.4   Comparison to Test Data From Reference 3
Reference 3 provides measured results of void fraction
and vessel pressure for a test vessel which was
partially filled with saturated water at high pressure
and then blown down through an orifice. The
configuration of the test vessel is shown in figure B3
as it appears in Reference 3. As the vessel
depressurizes, the saturated water inside the vessel
flashes into steam. The void fraction as a function of
height in the vessel at different pressures during the
blowdown provides a good test for the effect of slip
between water and steam as the steam tries to escape
from the vessel. Figure B4 compares the measured void

fraction as provided in Reference 3 at 10 seconds and at 40 seconds after initiation of the blowdown to those which were calculated by the thermal hydraulic computer program used to analyze the ___ _ _ auxiliary feed pump steam supply piping. The comparison shows that the slip model in the computer program is adequate to determine qualitatively the separation of steam and water which would have occurred during the June 9th transient at _____.

Figure B5 compares the rate of depressurization from Reference 3 to that calculated by the thermal hydraulic program used to analyze the __ _ __Auxiliary Feed Pump Turbine steam supply piping. The comparison indicates that a slightly more rapid depressurization is calculated than was measured; however, for both the pressure rate of change and the void fraction distribution, the agreement with the measured data is considered good. The lower calculated value for the pressure at 40 seconds is consistent with the higher void fraction which is calculated for that time.

B.5   Analysis of a Pipe Compression Wave

As a final check on results obtained from the thermal
hydraulic computer program, a long pipe at high
pressure and closed at one end was analyzed for the
effect of a sudden increase in pressure at the open
boundary. Superheated steam was used as the medium
inside the pipe. The analytic solution of this problem
requires that the shock front travel down the pipe at
the speed of sound and is reflected from the closed end
at twice its original magnitude. The speed of sound is
not an input to the thermal hydraulic program and must
be obtained from the solution of the fluid conservation
equations combined with the equations of state used by
the program. Consequently, the solution to this
problem is considered to be a good test of the fluid
dynamics as they are solved for the Davis-Besse June
9th transient particularly since opening the steam
admission valves in the __ __ __ auxiliary feed pump
piping (which admits high pressure steam from the steam
generators into the low pressure region of the
auxiliary feed pump steam piping to pressurize the
piping) is similar in nature to the sudden
pressurization of one end of the pipe as analyzed for
this problem. The configuration used for the test
problem is shown in Figure B6.

Results from the test problem are shown in Figure B7. These results indicate that the wave front which forms due to the sudden pressurization holds its shape and travels at a speed of about 1950 feet per second once it has diffused over a few control volumes. The speed of sound for superheated steam at 500 psia and 600 degrees Fahrenheit is given as 1860 feet per second in Reference 4. The reflected wave from the closed end of the pipe also behaves as expected. Consequently, the effect of the much slower pressurization which occurs at   when the valves in the feed pump turbine steam supply piping are opened on a slow ramp in time should be determined adequately by the thermal hydraulic computer program used for this analysis.
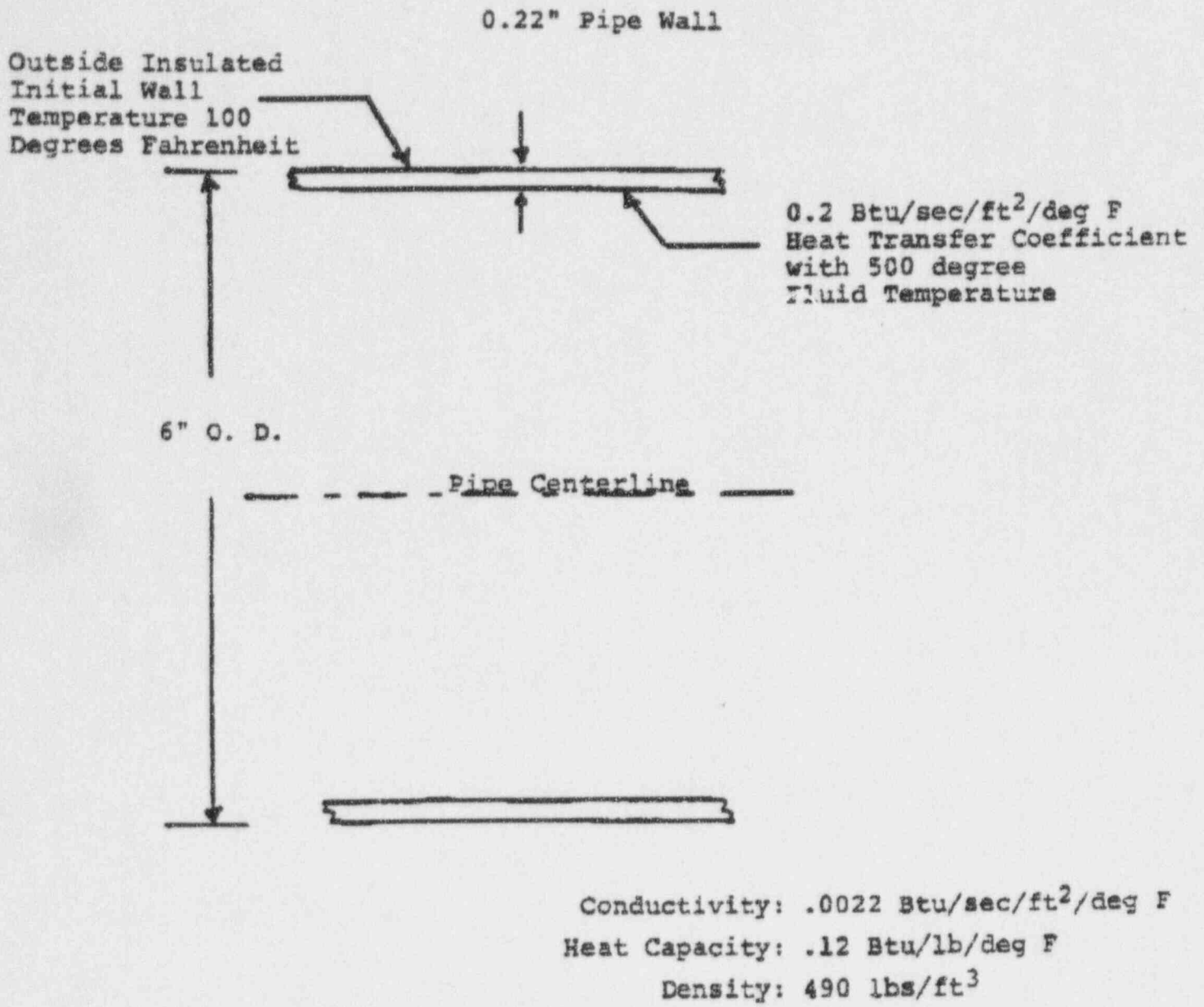
0.22" Pipe Wall

Outside Insulated
Initial Wall
Temperature 100
Degrees Fahrenheit

0.2 Btu/sec/ft^2/deg F
Heat Transfer Coefficient
with 500 degree
Fluid Temperature

6" O. D.

Pipe Centerline

Conductivity: .0022 Btu/sec/ft^2/deg F

Heat Capacity: .12 Btu/lb/deg F

Density: 490 lbs/ft^3

FIGURE B1

Schematic of Pipe Used for Thermal
Conduction Problem
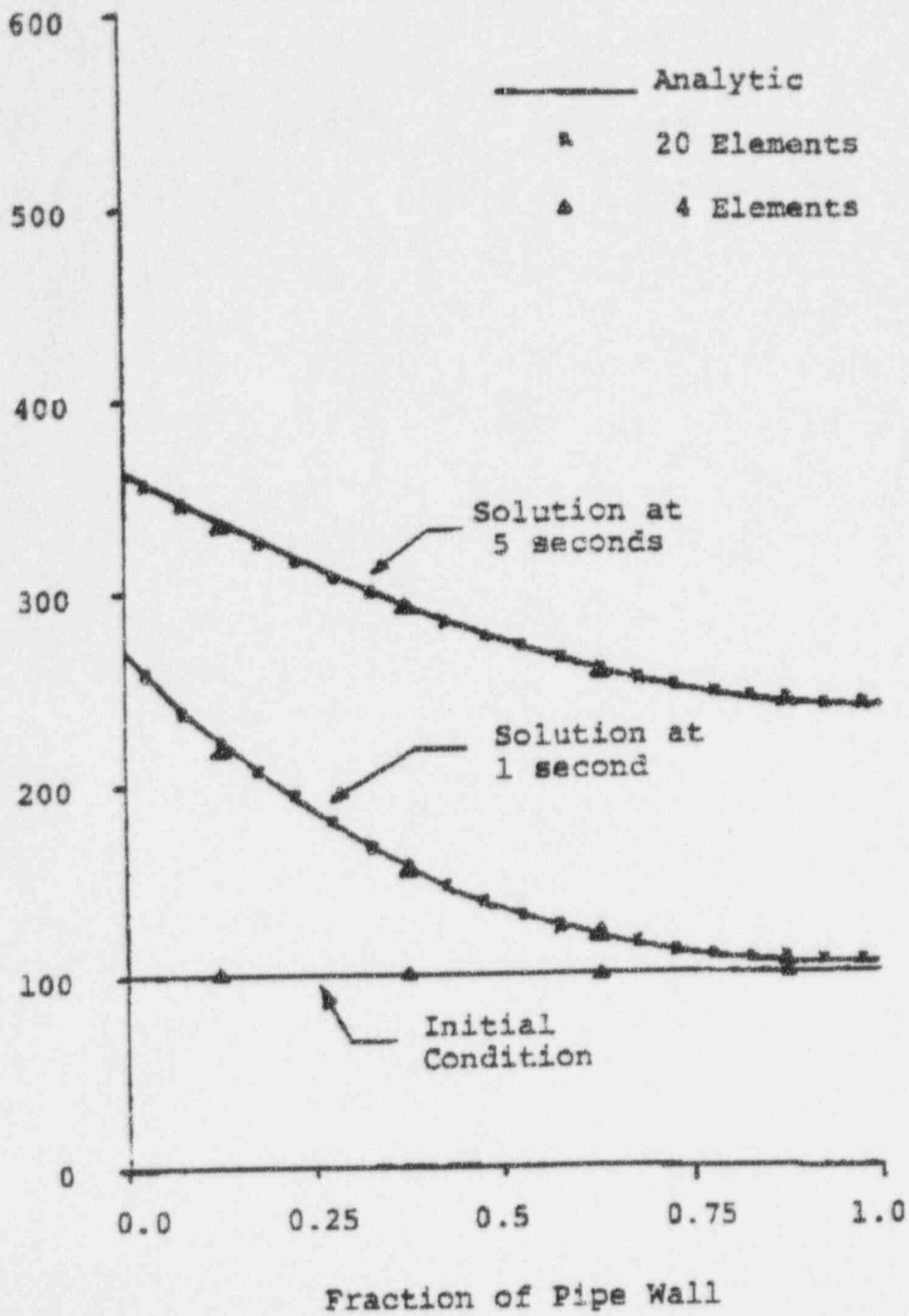
FIGURE B2

Solution for Heat Conduction
Through Pipe Wall

Test Configuration   Computer Model

Blowdown
Orifice

14 feet

1 foot

Blowdown
Valve

Suppression
Tank

14

15

13

Boundary
at
Atmospheric
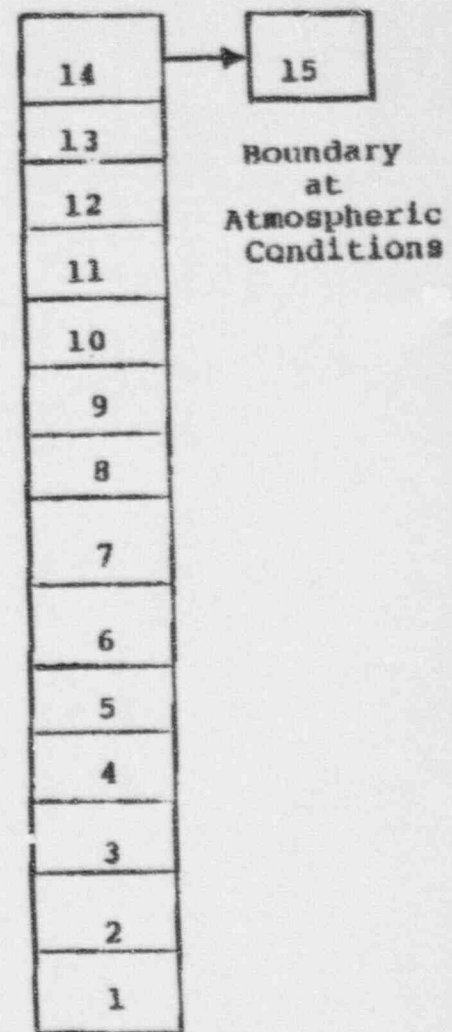Conditions

12

11

10

9

8

7

6

5

4

3

2

1

FIGURE B3
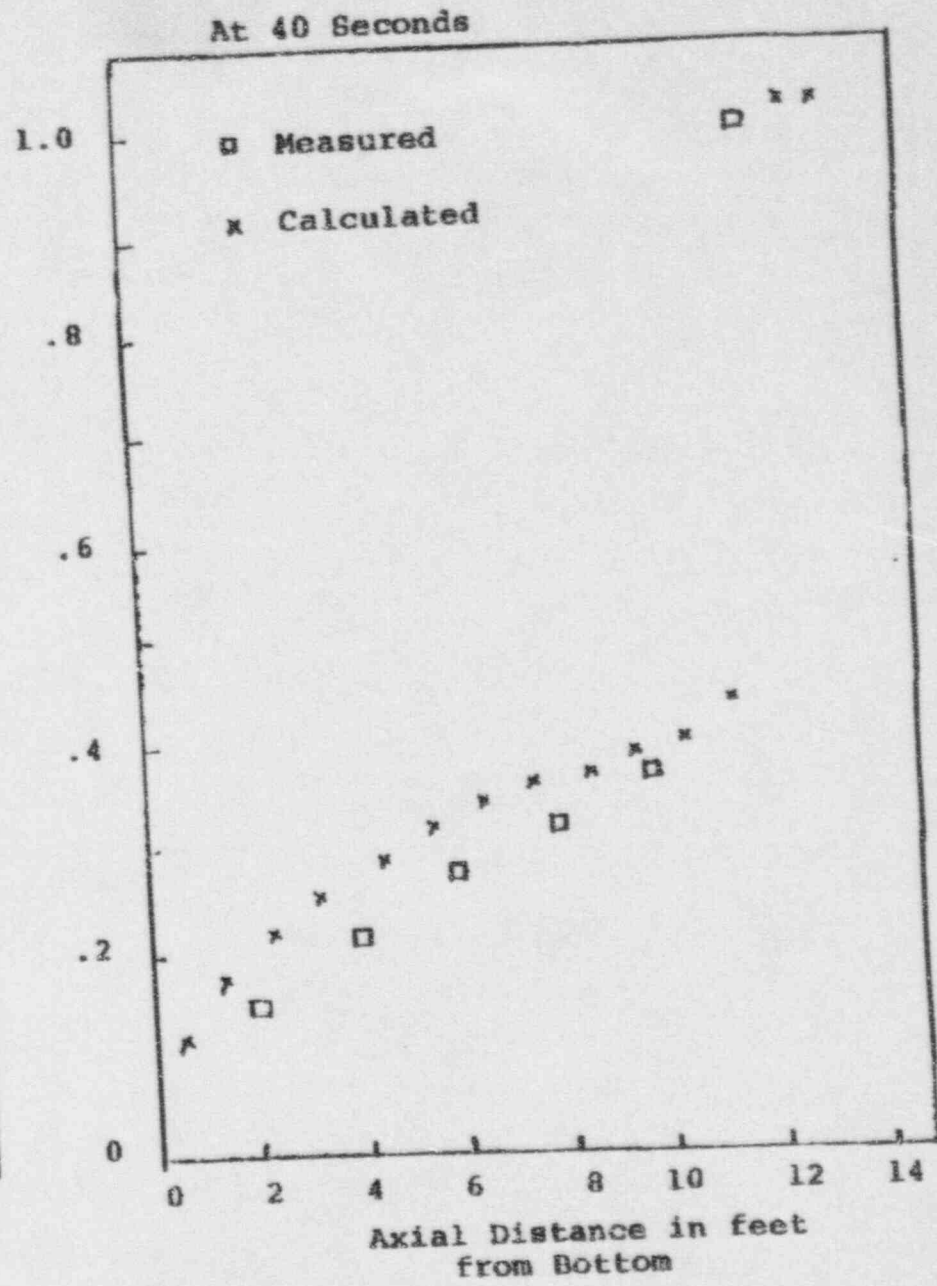
Test Configuration from Reference 3 and
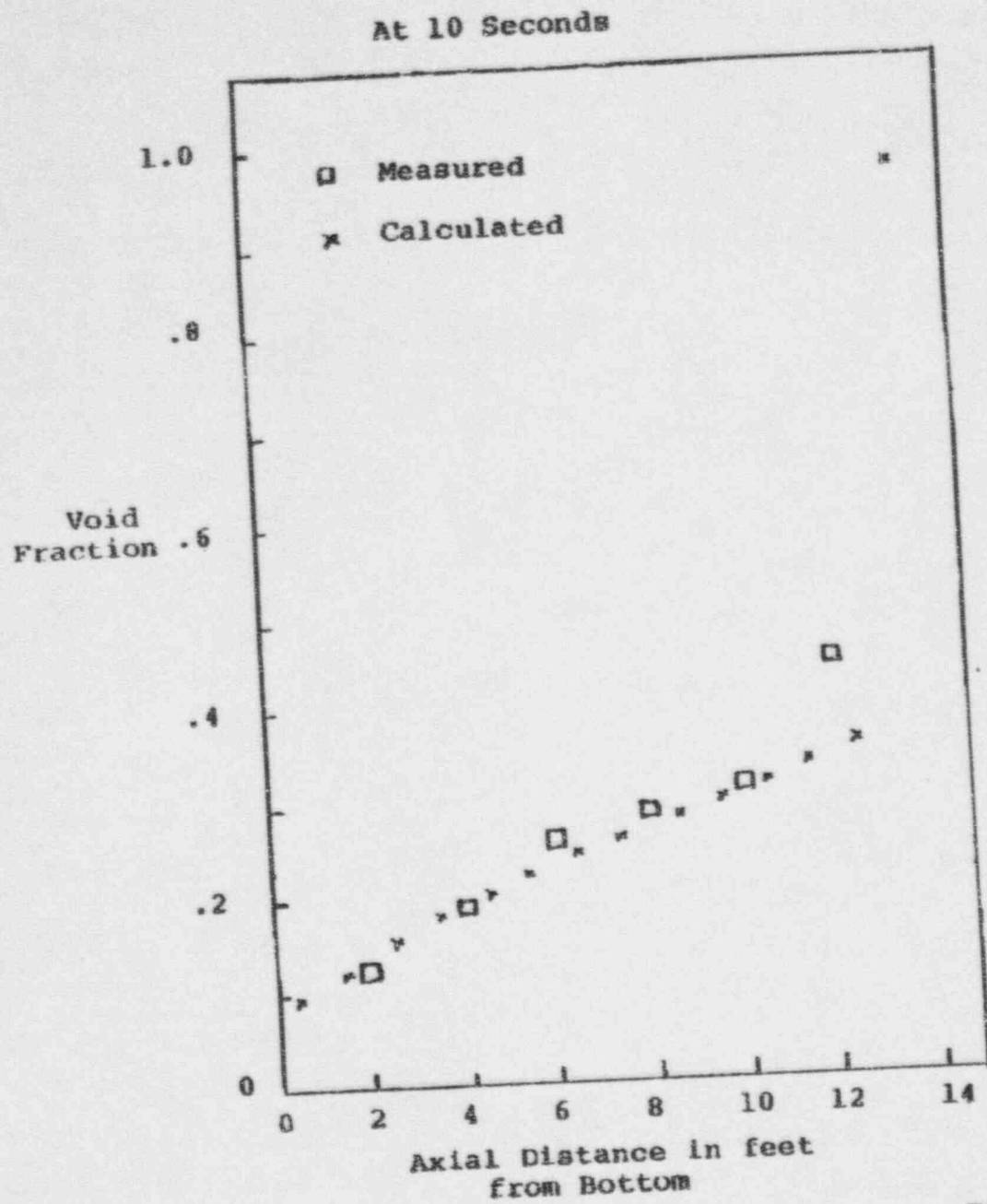Computer Model

FIGURE B4
Comparison of Calculated and Measured Voids
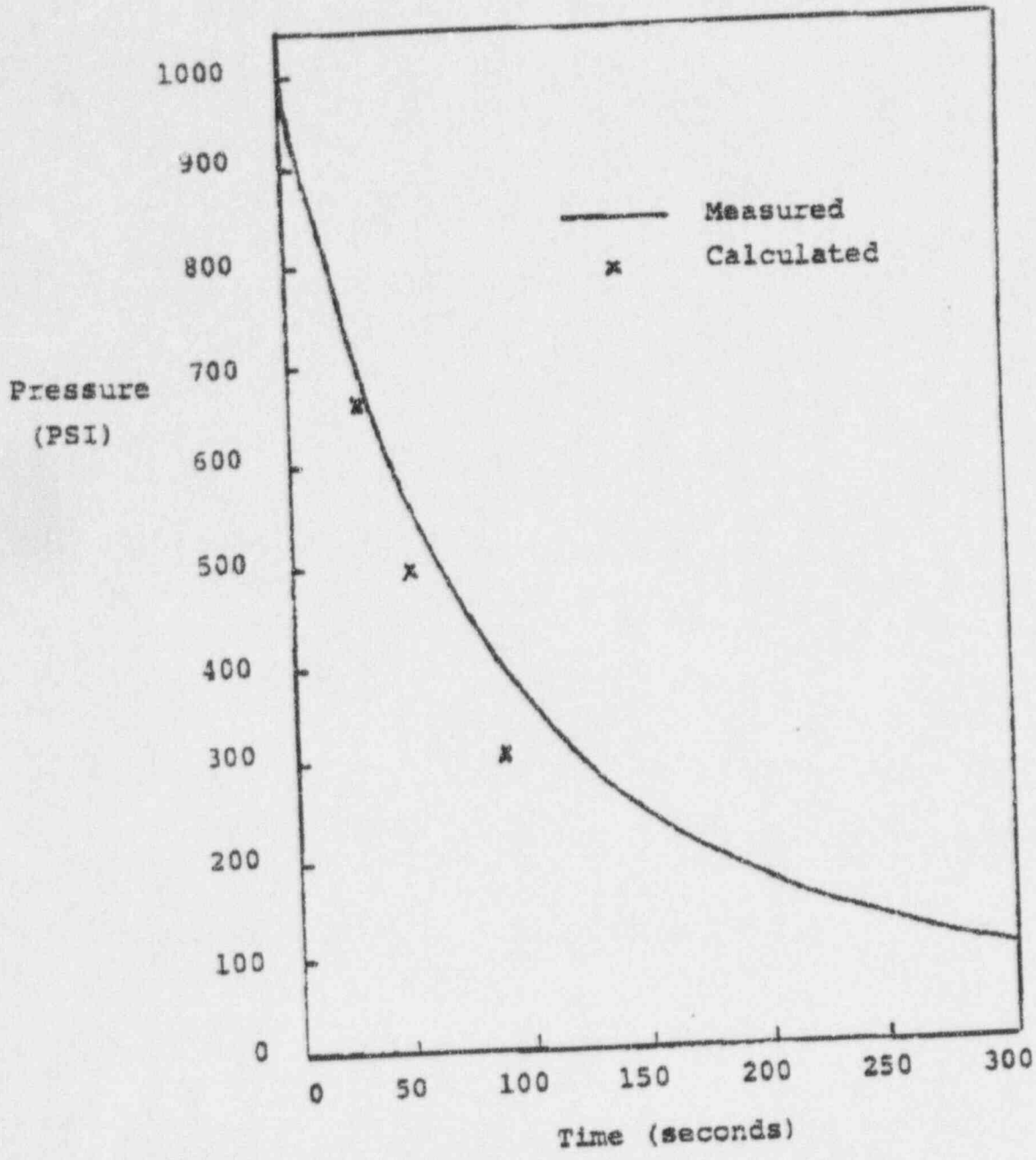for Test from Reference 3

FIGURE B5

Comparison between Measured and Calculated Pressure
for Test from Reference 3

Pipe Diameter: 2 feet
Initial Pressure: 500 psia
Initial Temperature: 600°F

Closed
at
End

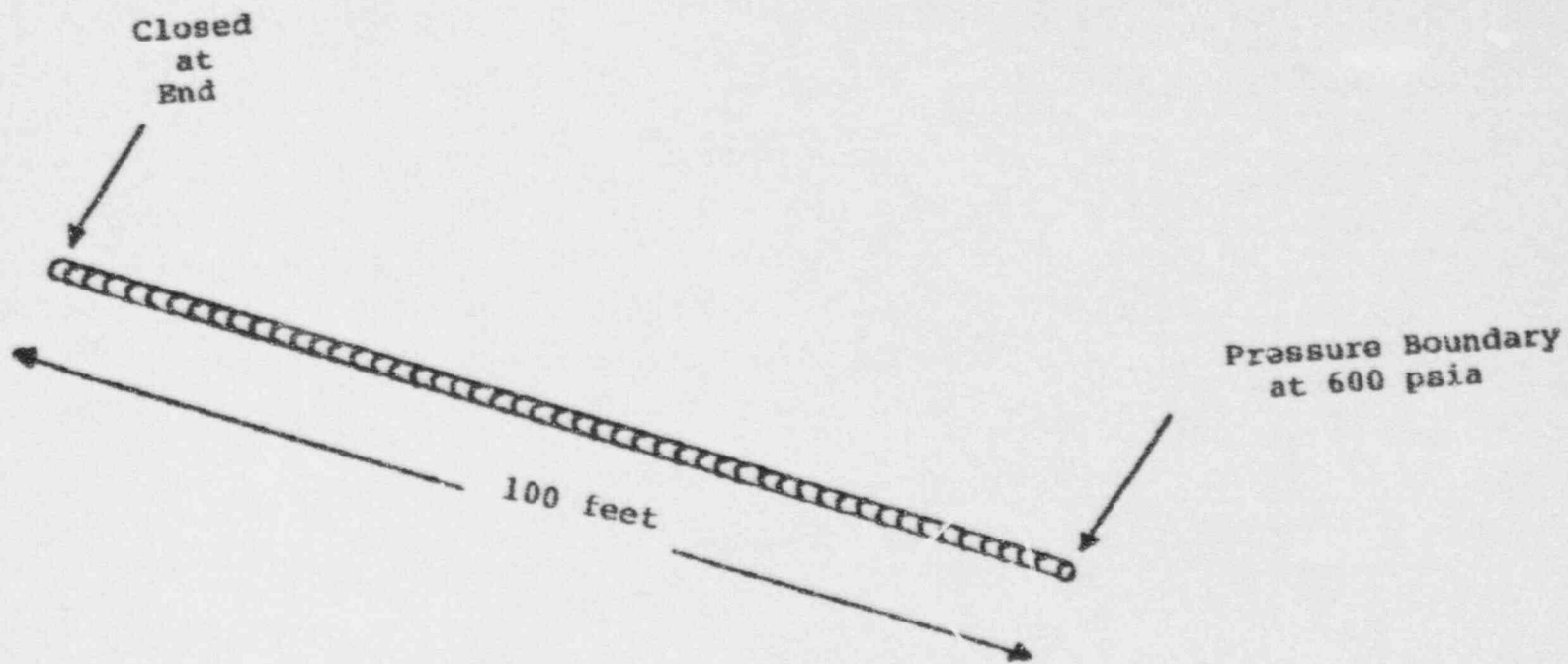Pressure Boundary
at 600 psia

100 feet

FIGURE B6

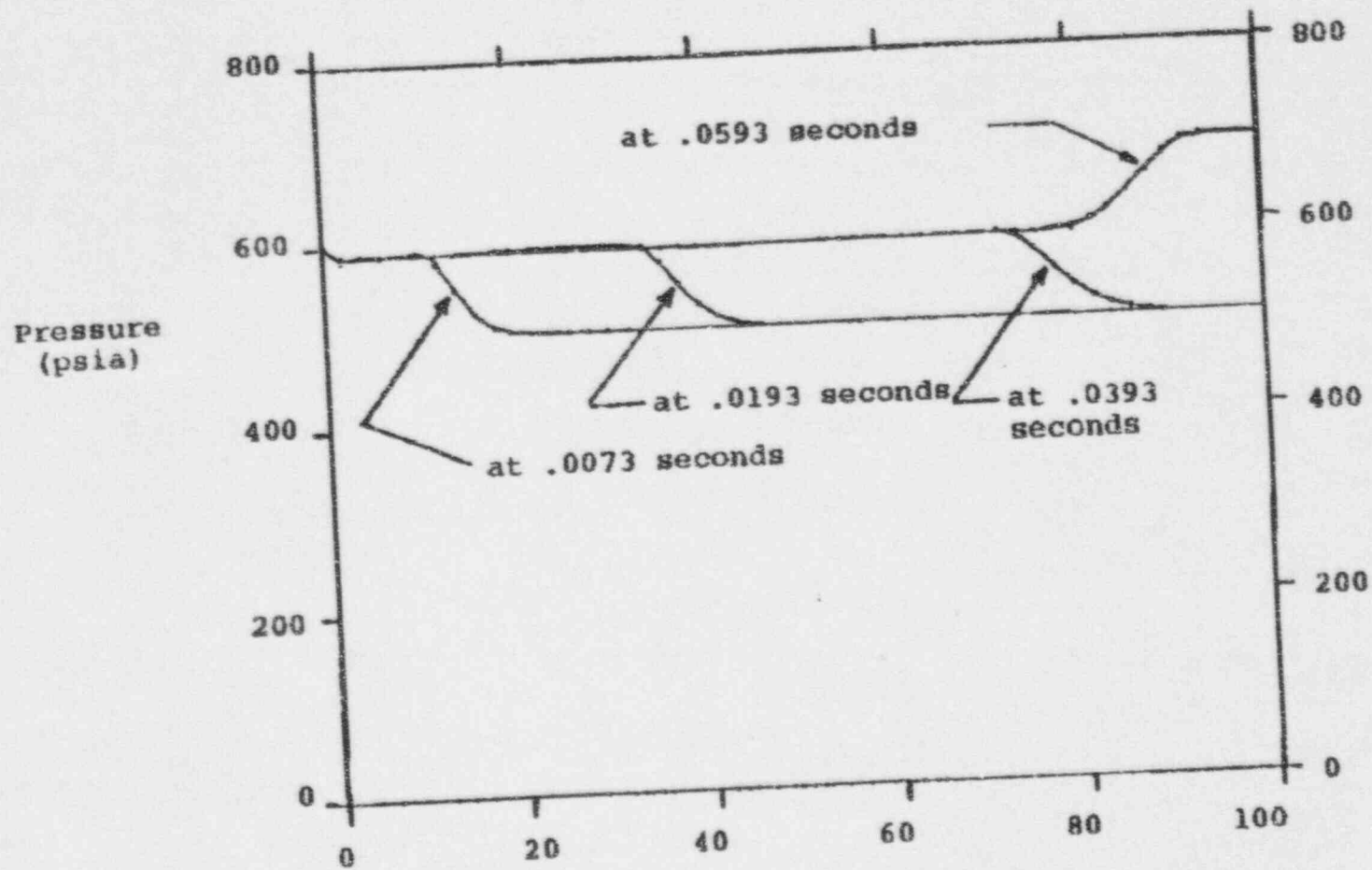Geometry Used for Pressurized Pipe Test Problem

FIGURE B7

Pressure Distribution at Various Times
for Pipe Pressurized at End

Enclosure 3

Paper Presented to ASME/IEEE
Power Generation Conference

in the connector representing the pump is modified accordingly. In the second case, for example after a pump trip occurs, the coastdown of the pump depends on the interaction of the pump with the fluid and a dynamic torque balance on the pump shaft. In the second case, the solution of equations in addition to the fluid dynamic equations will be required to represent the pump behavior. The rate of change of the speed of the pump is given by the torque divided by the rotary inertia of the pump shaft assembly.

$$\omega = \frac{t}{I} \qquad (12)$$

where: t is the net torque on the pump
I is the rotary inertia of the pump shaft assembly

The net torque on the pump includes the torque due to the pump motor, the torque applied by the fluid, torque from losses in the bearings, and torque due to losses from the fluid.

$$t = t_e - t_f - t_b - t_{fl} \qquad (13)$$

where: t_e is the torque applied by the motor

$t_f = \Delta P \dfrac{W}{\rho \omega}$ is the fluid torque

$t_b = f_b \dfrac{P_{ref}}{\omega_{ref}} \left(\dfrac{\omega}{\omega_{ref}} \right)^2$

$t_{fl} = \dfrac{(1 - \eta - f_b) P_{ref}}{\omega_{ref}} \left(\dfrac{W}{W_{ref}} \right)^2$

ΔP is the pressure difference across pump
W is the mass flow rate through pump
P_{ref} is the power at full speed
f_b is a bearing loss coefficient
η is the pump efficiency

Valves
Valves are included as flow areas which change as a function of time. The parameters in the momentum equation which are affected include the inertial length and the flow loss coefficient. Reducing the area of a connector will increase the pressure drop across the connector and will cause the flow rate through the connector to decrease. Imposing a change in a flow area as a function of time on a flow connector is straightforward and is easily handled directly in the solution for the fluid equations, similar to the imposition of a time dependent pump speed on the fluid solution as discussed previously. However, in the case of a check valve, dynamic equations which determine the position of the check valve disk based on a force balance on the disk must be added to the fluid solution in a manner similar to the solution required for the pump speed when the speed is affected by the fluid conditions. A typical swing check valve geometry is shown in Figure 2 and the equation of motion for the disk is given below.

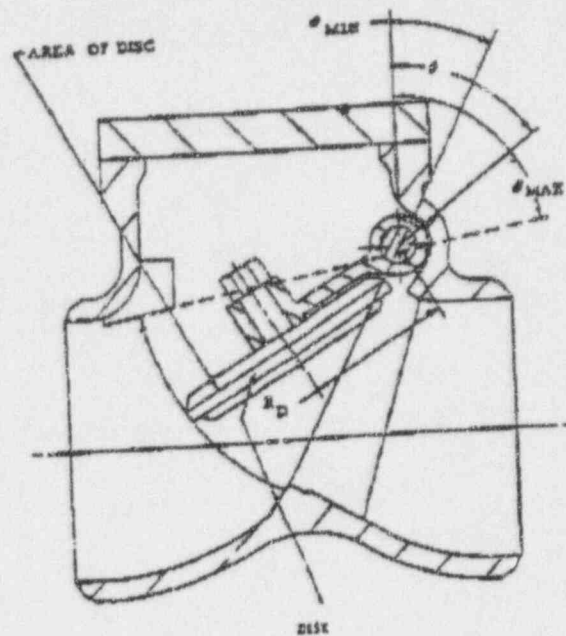$$\ddot{\Theta} = \frac{t}{I} \qquad (14)$$

FIGURE 2
Typical Check Valve Geometry

where: Θ is the angle of the disk
t is the net torque on the disk assembly
I is the rotary inertia of the disk

The net torque tending to rotate the disk includes the fluid forces, the buoyant weight of the disk, friction in the shaft, and spring load if the check valve has a spring.

$$t = t_f + t_w + t_b + t_s \qquad (15)$$

where: $t_f = \Delta P \, A_D R_D$ is the fluid torque on the disk

$t_w = W_D R_{cg} \sin(\Theta - \Theta_{fh})$ is the torque due to weight of the disk

$t_b = \mu R_s R_{cg} M_D \dot{\Theta}^2$ is the torque due to friction on shaft from centrifugal load on the disk

μ is the friction coefficient on the shaft

$t_s = K_s R_s \sin(\Theta - \Theta_s)$ is the torque due to a spring

A_D is the area of the disk

R_D is the moment arm from the shaft to the center of the disk

W_D is the bouyant weight of disk assembly

M_D is the mass of the disk assembly

R_{cg} is the moment arm from the shaft to the center of gravity of the disk assembly

Θ_{fh} is the angle at which disk hangs freely

R_s is the radius of the shaft

4

K_s is the spring constant

R_s is the moment arm from the shaft to the spring

θ_s is the angle at which the disk contacts the spring

Conduction Heat Transfer

A conservation of heat flux approach is used to solve for the transient temperature distribution in the metal parts of the geometry by dividing that geometry into a number of control volumes and requiring that the net heating rate in each volume satisfy the energy conservation equation. The net heat rate for each volume is written as a function of the temperature at the centroid of that volume and the resulting algebraic equations are solved implicitly. The heat conduction equation can be written in the following form.

$$\rho C \frac{\partial T}{\partial t} = \nabla \cdot J + S \tag{16}$$

$$J = -k \nabla T \tag{17}$$

where: J   is the thermal heat flux
S   is the heat source per unit volume
k   is the thermal conductivity
T   is the temperature
ρ is the density
C   is the specific heat capacity
t   is time

Equation (16) represents the condition that the rate of change of temperature at a point depends on the rate of heat flow to that point and the rate of heat generation at that point. Equation (17) is the definition of the heat flux, which is proportional to the temperature gradient and flows from higher temperature to lower temperature. The conductivity is just the proportionality constant between heat flux and the temperature gradient. By substituting Equation (17) into Equation (16) and assuming the thermal conductivity is not dependent on position, the normal steady state heat conduction is obtained.

$$\rho C \frac{\partial T}{\partial t} + k \nabla^2 T = S \tag{18}$$

The numerical approach used to solve the heat conduction equation is based on Equations (16) and (17) directly rather than on the heat conduction equation given in Equation (18). By dividing the region of solution into a large number of volumes which are connected to each other by heat flow paths or connectors, the method integrates Equation (16) over each volume and describes the heat flow in each connector in terms of the temperature at the center of the connected volumes using the following numerical approximation for Equation (17).

$$J_k = (T_i - T_j) / R_k \tag{19}$$

$$Q_k = AH_k J_k \tag{20}$$

where: J_k is the heat flux in connector k between nodes i,j

T_i is the temperature at node i

T_j is the temperature at node j

R_k is the thermal resistance for connector k

Q_k is the total heat flow in connector k

AH_k is the heat transfer area of connector k

The integrated form of Equation (16) becomes:

$$\rho C \, Vol_m \frac{T_m^{n+1} - T_m^n}{\Delta t} + \sum_{\substack{all\ k \\ on\ node\ m}} AH_k (T_i - T_j)/R_k = S_m Vol_m \tag{21}$$

where: S_m is the heat generation per unit volume in volume m

Vol_m is the volume of control volume m

T_m^n is the temperature in volume m at the beginning of the time step

T_m^{n+1} is the temperature in volume m at the end of the time step

There will be one equation like Equation (21) for each volume in the structure. The total set of equations can be represented by a single matrix equation of the form:

$$A \, T = B \tag{22}$$

where: A is the matrix of coefficients in Eq. (21)
T is the vector of unknown temperatures
B is the right hand side vector

Boundary conditions must be imposed on Equation (22) to represent the effects of boundary conditions on the geometry being analyzed. Three different types of boundary conditions are provided. These boundary conditions are treated as surface connectors which contribute to Equation (22) as additional heat flows as follows.

1. Temperature specified on boundary. The additional heat flow represents a resistance path between the node at the centroid of volume m and the surface which is at a specified temperature, TB.

$$Q_k = AS_k(T_m - TB) / RS_k \tag{23}$$

where: AS_k is the heat transfer area of the path

RS_k is the resistance between the node the volume centroid and the surface

2. Heat flux specified on boundary. The additional heat flow is specified directly by the heat flux on the boundary, JB.

$$Q_k = AS_k \, JB \tag{24}$$

3. Heat transfer coefficient specified on boundary. The additional heat flow is represented by the resistance path between the center of volume m to the surface which is at temperature TB with a heat transfer coefficient, HTC.
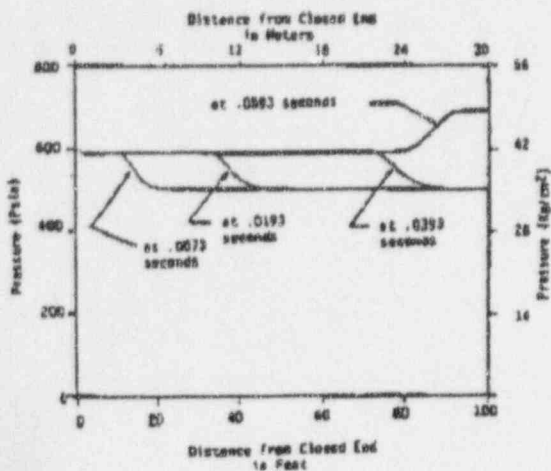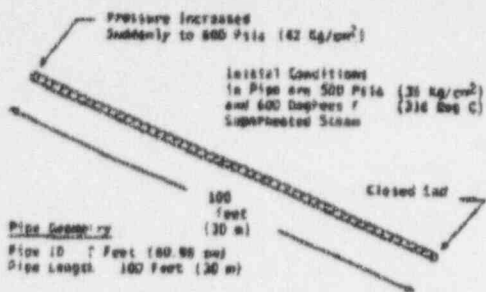
5

FIGURE 3
Test Problem for Propagation of a Pressure
Wave Front in a Pipe

$$Q_k = AS_k(T_m - TB) / (1/HTC + RS_k) \qquad (25)$$

The specified parts of Equation (21) are transferred
to the B vector side of the equation and the unknown
temperatures are obtained by solving the resulting
matrix equation.

DESCRIPTION OF COMPUTER PROGRAM

The analytic approach described above has been
incorporated into a computer program to simplify the
evaluation of pipe motion during transients. A
considerable number of Pre-and Post-Processing
features have been developed to allow input data to
be entered easily and to allow the results to be
interpreted quickly. The solution technique used has
been optimized over the last several years to
increase the efficiency of the calculations to the
point where most transients which have been analyzed
will run within a few hours on an IBM PC computer or
compatible. Simple transients will run in a few
minutes.

COMPARISON TO ANALYTIC RESULTS

Results obtained using the approach outlined above
were compared to analytic solutions for two simple
geometries. The first of these was a sudden
compression in a pipe containing pressurized steam,
similar to what might occur upstream of a suddenly
closed valve. This problem tests the propagation
characteristics of the numerical approach for the

fluid solution. In the second comparison, the
transient heat conduction was calculated for a pipe
wall given a specific heat transfer coefficient and
an internal fluid temperature. The second case tests
the numerical approach used for the heat conduction
solution.

For the first case, the analytic solution predicts
the establishment of a wave front at the end of the
pipe which is suddenly pressurized and the wave front
propagates along the pipe at the speed of sound,
reflecting from the closed end of the pipe at twice
the incoming amplitude. The geometry used in the
analysis and a description of the results obtained
are provided in Figure 3. The results indicate that
the speed of propagation of the wave front obtained
from the numerical technique agrees well with that
published in Reference 2. The propagation velocity
of a pressure pulse obtained from the numerical
solution is only a function of the equations of state
and the conservation equations employed, and is not
explicitly provided to the solution technique.

The geometry and a comparison of the results obtained
for the heat conduction problem using the numerical
technique to an analytic solution are shown in
Figure 4. In this case, the numerical technique
provides accurate results for the temperature
distribution across the pipe wall with as few as four
volumes provided across the pipe wall thickness.

COMPARISON TO TURBINE TRIP

The approach outlined above was used to calculate the
transient pressure response for a turbine trip at a
nuclear power plant. The turbine interceptor valves
used to isolate the turbine from steam flow are fast
acting valves which close in a fraction of a second
and can set up a rapid pressure increase in the
piping upstream of the valve.

Figure 5 shows a schematic of the system which was
analyzed. The steam generator, which supplies steam
to the turbine, will react to the pressure waves
which propagate through the pipe and the complete
steam generator was included in the model. The heat
transfer in the steam generator also affects the
response and was included in the model. In the
particular case analyzed here, pressure measurements
in the piping were not available; however, the
absolute pressure in the steam generator and the
water level which is based on pressure differential
measurements across a part of the steam generator
were recorded. The comparison of calculated results
to measured results for the pressure in the steam
generator is shown in Figure 6 and indicates good
agreement. The small pressure pulses recorded in the
steam generator are a response to the larger pressure
swings which occur in the piping between the steam
generator and the interceptor valves. Calculated
pressure at the interceptor valve is included in
Figure 6.

The recorded water level in the steam generator is
shown in Figure 7. This measurement actually
measures the difference in pressure between two
points in the steam generator and consequently
reflects the pressure oscillations produced in the
piping. Also shown in the figure is the calculated
mass flow rate leaving the steam generator. The
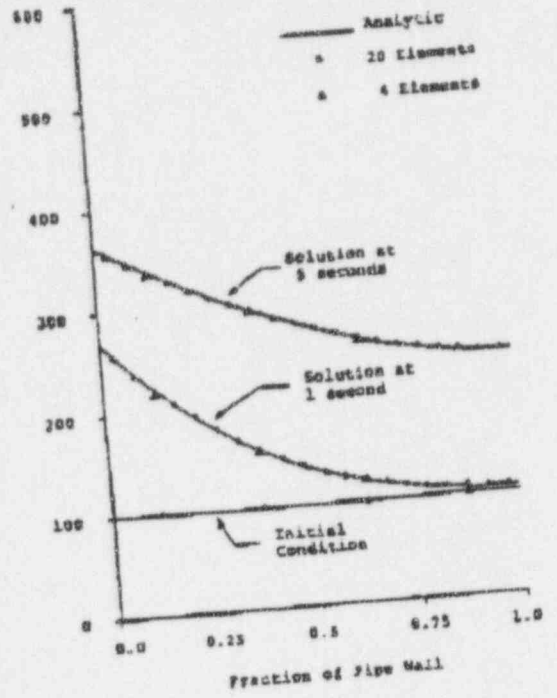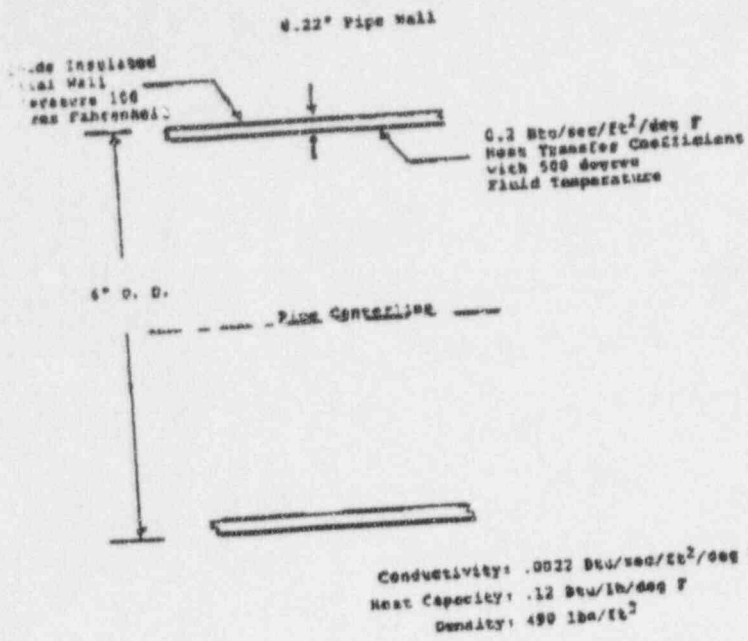measured water level and the calculated mass flow

FIGURE 4
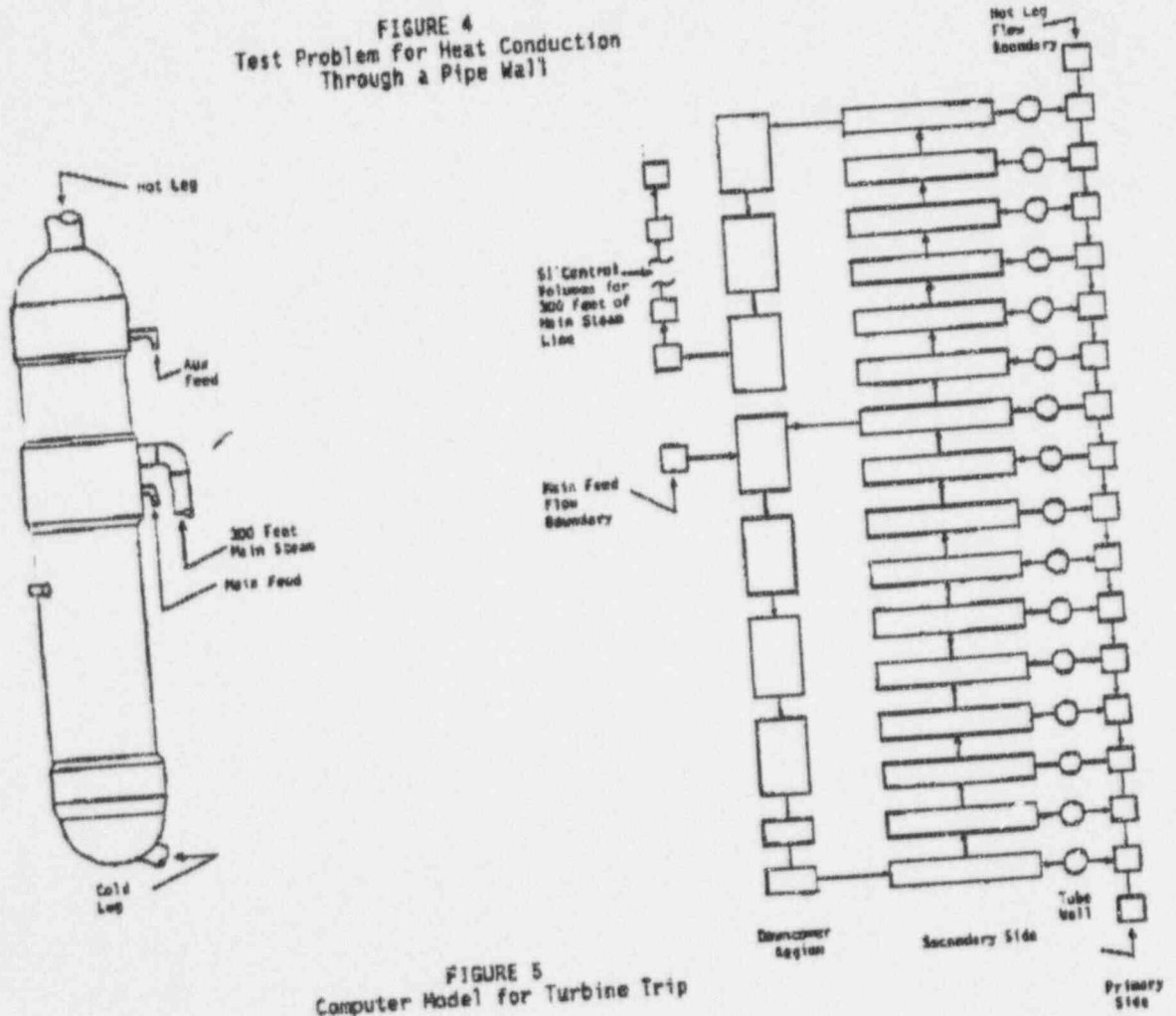Test Problem for Heat Conduction
Through a Pipe Wall

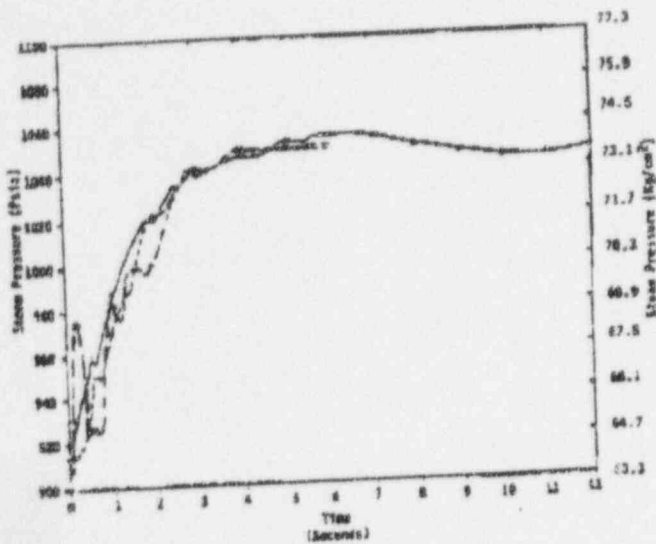FIGURE 5
Computer Model for Turbine Trip
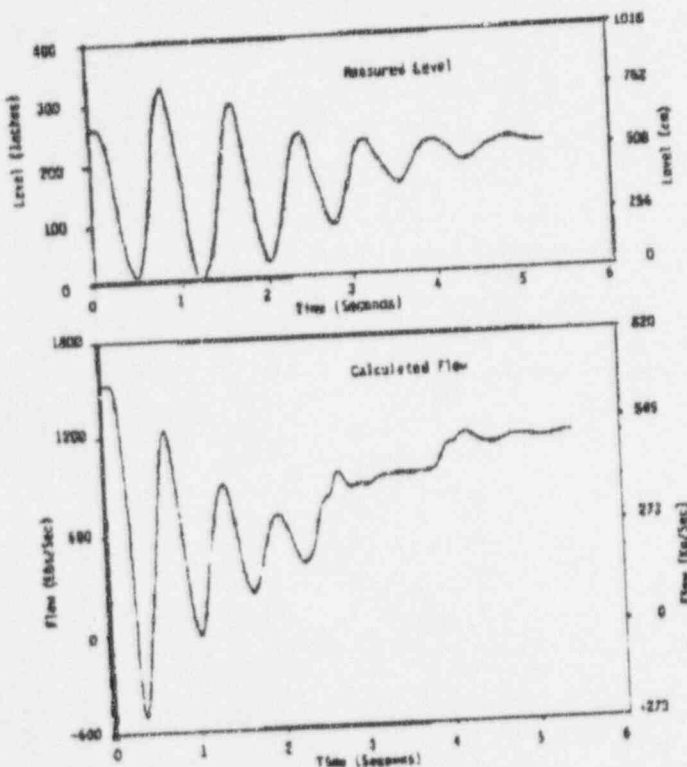
FIGURE 6
Pressure Comparison for Turbine Trip

FIGURE 7
Comparison of Steam Generator Flow to
Measured Water Level for Turbine Trip

rate respond at about the same frequency. The reason
the steam generator flow remains high at the end of
the transient is because safety valves and turbine
by-pass valves opened as a result of the transient.

COMPARISON TO PIPE MOTION DATA

Transient data for pipe motion at power plants is
difficult to obtain since measurements are not
normally available for severe transients which cause
significant pipe motion. However, the magnitude of
the motion can sometimes be inferred from
consequential damage, such as deformation of piping
supports or from scratch marks on piping or torn
insulation. Several plant transients have been
analyzed by the approach described above and results
consistent with the observed damage have been
obtained. Two such incidents which have been
analyzed are described below.

1. Two recirculation pumps are aligned in parallel.
    In order to allow the pumps to be operated
    individually, check valves are installed at the
    discharge of each pump to prevent the flow from
    a single running pump from passing through the
    secured pump. When both pumps are running and
    one of them is tripped, the check valve at the
    discharge of the tripped pump will close and a
    waterhammer event occurs. In the case analyzed,
    significant deformation of a pipe support near
    the suction side of the tripped pump occurred.
    An analysis of the transient was used to
    accurately predict the deformation of the hanger
    and to determine if the redesign of the hanger
    was adequate.

2. A disk in a control valve broke from its
    attachment support and freely floated within the
    valve body. The design of the valve was such
    that the disk was unstable in this condition.
    The interaction of the disk motion and the
    resulting pipe response set up a severe
    vibration transient in the piping system,
    damaging several supports on the piping system.
    An analysis of the transient was used to obtain
    piping loads which were consistent with the
    observed damage and the resulting calculated
    stresses in the pipe were evaluated to
    demonstrate the integrity of the piping.

CONCLUSION

The analytic approach described above, and its
implementation in a computer program which is easy to
use and runs on a personal computer, has proven to be
a useful and practical tool in design work and in
evaluating power plant problems.

REFERENCES

1. Porsching, T. A., Murphy, J. H., Redfield, J. A.,
   and Davis, V. C., "Flash-4; a Fully Implicit
   Fortran IV Program for the Digital Simulation of
   Transients in a Reactor Plant", March 1969.
   WAPD-TM-840, Bettis Atomic Power Laboratory.

2. C. A. Meyer, R. B. McClintock, G. J. Silvestri,
   and R. C. Spenser, Jr., "ASME Steam Tables, Fifth
   Edition"

TRANSIENT TWO-PHASE BLOWDOWN PREDICTIONS OF AN INITIALLY STAGNANT SATURATED LIQUID STEAM IN A VESSEL USING TRAC-PF1

YASSIN A. HASSAN *The Babcock & Wilcox Company, Nuclear Power Division*
P.O. Box 10935, Lynchburg, Virginia 24506-0935

Comparisons of the predictions of the best-estimate pressurized water reactor TRAC-PF1/MOD1 computer code to data of the General Electric level swell tests were performed. Various time-step sizes and nodalization schemes were employed. With appropriate time-step size, void fraction distributions predicted by TRAC compared favorably with the void fractions inferred from the measured data. Nonphysical oscillations in spatial void profiles were observed when a large time step was used. Comparisons of TRAC predictions with results obtained using three codes of the RELAP family were performed.

INTRODUCTION

Simulations of two small vessel blowdown tests were performed using the best-estimate pressurized water reactor (PWR) TRAC-PF1 (Version 11.6) computer code.[1] The primary objective of these experiments, conducted at General Electric Company (GE) (Refs. 2 and 3), was to investigate blowdown phenomena such as two-phase mixture level swell and to investigate void fraction distributions during blowdown. The two-phase blowdown phenomenon is a subject of great interest to both the chemical and power industries. It is particularly pertinent to steam-water boilers and to pressurized and boiling water nuclear reactor systems.

The GE swell blowdown facility consisted of a vertical pressure vessel, a blowdown line containing an orifice, and a suppression tank at atmospheric conditions. A schematic drawing of the test section is depicted in Fig. 1. Detailed descriptions of the test are presented in Refs. 2 and 3. The pressure vessel was a 4.27-m- (14-ft) long and 0.3048-m-(1-ft) diam vertically oriented cylindrical tank. Instrumentation included six differential pressure (DP) cells spaced at equal axial intervals in the vessel. The measurements obtained from these DP cells were used to infer the void fraction distribu-
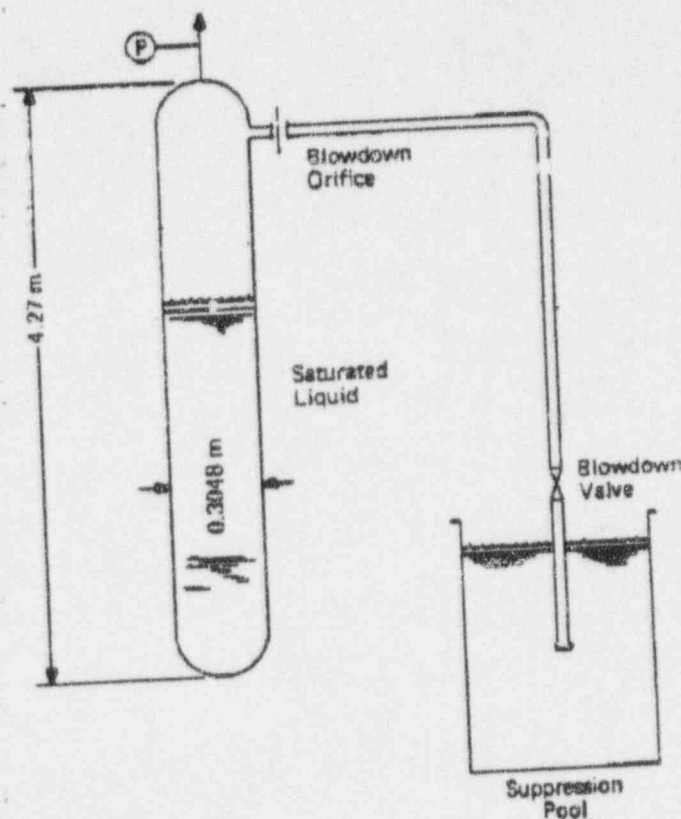

Fig. 1. Schematic of GE level swell test.

tion as the vessel was blown down from its initial state, partially filled with saturated water at ~6.90 MPa (1000 psia).

This study presents two simulations of two GE level tests using the TRAC-PF1/MOD1 computer code. Comparisons between the TRAC-PF1 predictions and the experimental measurements are also presented.

TRAC MODEL DESCRIPTION

The TRAC-PF1/MOD1 computer code was developed at Los Alamos National Laboratory to calculate the thermal-hydraulic responses in PWRs for various accident and transient conditions. TRAC-PF1/MOD1 solves the six conservation equations describing two-phase flow, using constitutive relationships to model the phenomena that govern mass, momentum, and energy exchange between the phases. These relationships play a major role in the code predictions. The numerical solution scheme used to solve the conservation equations for two-phase flow is carefully formulated to avoid nonphysical oscillations. The stability-enhancing two-step method used for one-dimensional flow eliminates the material courant stability limit for one-dimensional components.

Fluid system modeling using TRAC-PF1/MOD1 is accomplished by constructing modules to describe the various components in the system and configuring the component modules in a manner that best describes the system. Component models available in TRAC-PF1/MOD1 include PIPE, TEE, STEAM GENERATOR, PUMP, BREAK, FILL, and other components necessary to model a PWR system. The basic model used to simulate the GE level swell tests uses a 14-cell PIPE component to model the vessel, a BREAK component to model the blowdown orifice, and a dummy FILL component to provide the remaining boundary conditions. This model is illustrated in Fig. 2.

Vessel top and bottom break locations using various blowdown orifice sizes were considered in the GE level swell tests. In this study, one blowdown test at each location was simulated using the TRAC-PF1 code. Test No. 1004.3, a top break, was simulated first. Th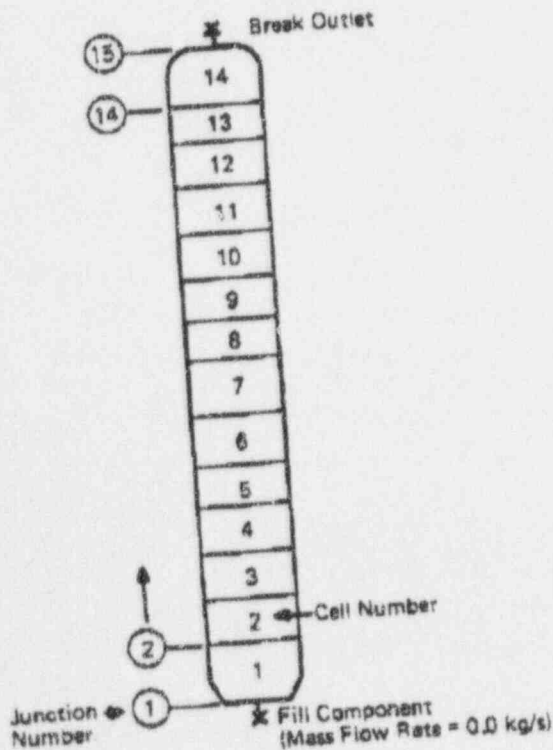e orifice used in this test was 0.009525 m ($\frac{3}{8}$ in.) in diameter. The saturated liquid level was 3.17 m (10.4 ft) at 6.97 MPa (1011 psia). The second simulation, a bottom break, was performed using the same orifice size. This case was initialized with 3.08 m (10.1 ft) of saturated liquid at 6.93 MPa (1005 psia). The transients were initiated from this stagnant initial condition by activating the break junction at time zero.

PREDICTIONS AND COMPARISON WITH DATA

Top Blowdown Test

The top blowdown test was simulated using TRAC-PF1/MOD1. The TRAC prediction of the vessel pressure transient, obtained using the homogeneous friction factor option with an additive loss coefficient K of 0.28 at the break junction, is compared against the measured pressure in Fig. 3. The TRAC predictions using this friction factor compare favorably with the data. The results of two additional cases, one with no additive loss coefficient at the break and one with an additive loss coefficient of 1.0, are also presented in Fig. 3. As expected, TRAC underpredicted the transient pressure when break orifice losses were neglected, and overpredicted the transient pressure when an additive loss coefficient of 1.0 was used.

The transient void fraction distribution is strongly dependent on interfacial momentum exchange between the liquid and steam phases. With appropriate time-step size and spatial detail, transient void fraction distributions predicted by

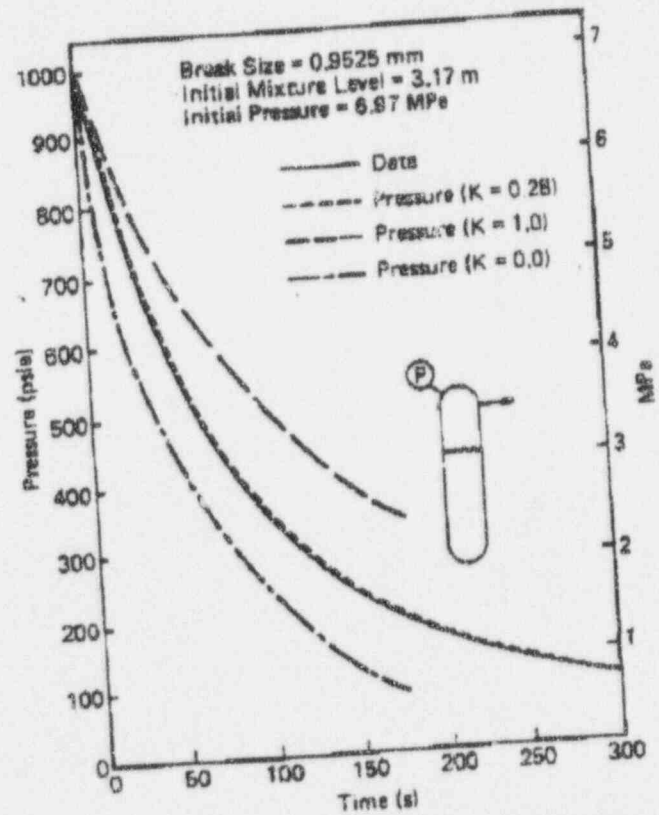Fig. 2. TRAC-PF1 noding for the GE small vessel blowdown.

Fig. 3. Comparison between the computed and the measured depressurization of GE level swell test 1004-3.
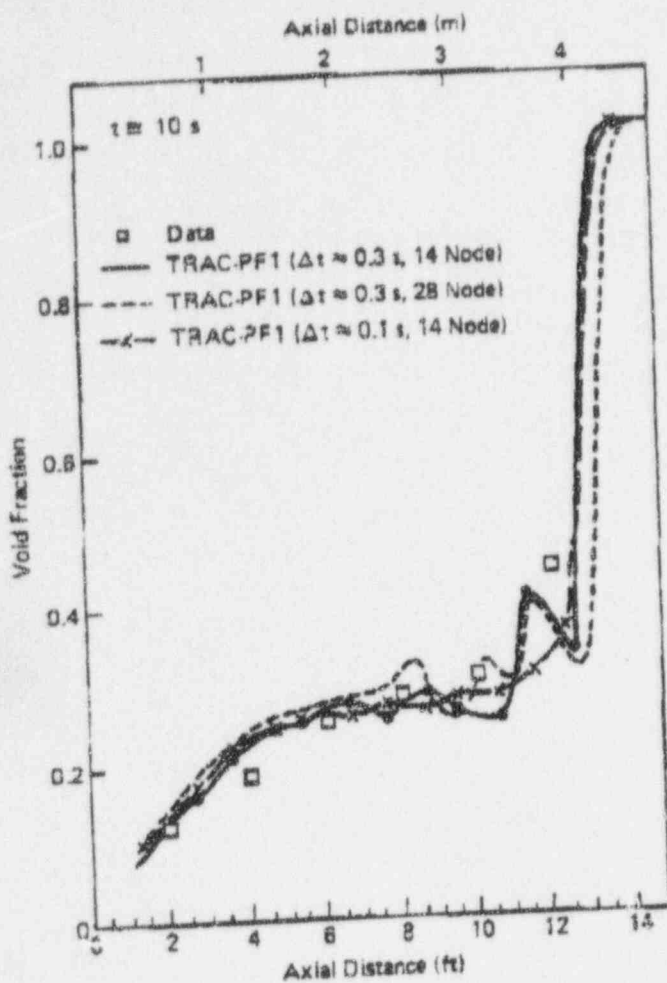
Fig. 4. Comparison between the computed and measured void fractions at transient time $t = 10$ s for test 1004-3.
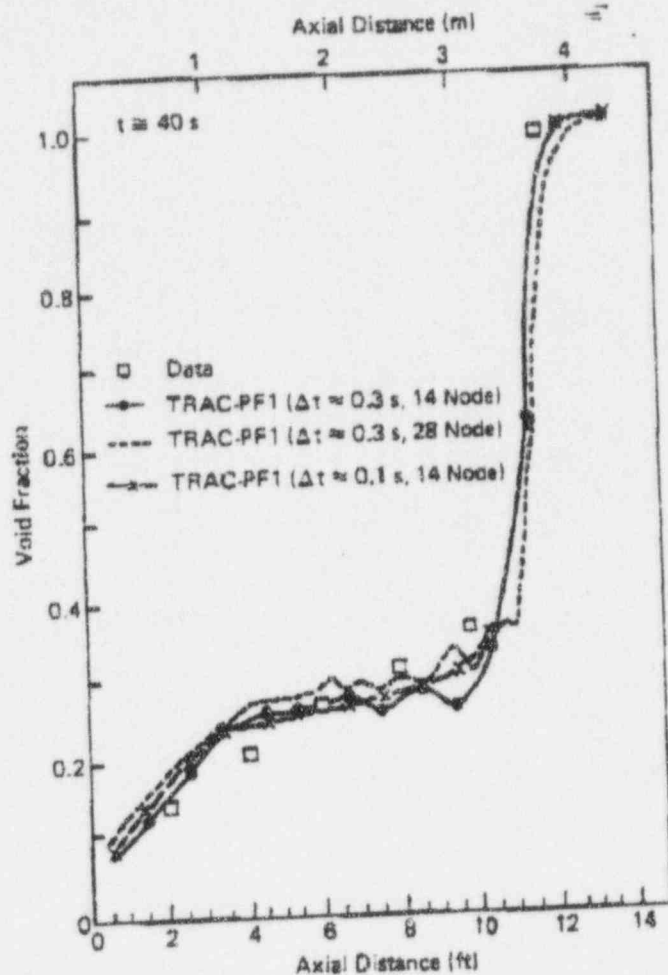

Fig. 5. Comparison between the computed and measured void fractions at transient time $t = 40$ s for test 1004-3.

TRAC-PF1 compare favorably with the void fraction distributions inferred from the measured data. Predicted and measured void fraction distributions obtained at 10, 40, 100, and 160 s after rupture are presented in Figs. 4 through 7, respectively. Nonphysical oscillations in the spatial void profiles were observed when a time step of 0.3 s was used. The oscillations were eliminated by decreasing the time step to 0.1 s. An increase in the number of computational cells used in the vessel model from 14 to 28 did not eliminate the oscillations. It is suspected that these time-step-related oscillations result from the explicit velocity dependence in the friction factor function forms and the strong void fraction dependence in the interfacial shear correlations.

The TRAC prediction of the void fraction distribution at 100 s after rupture is compared with experimental results and predictions obtained using RELAP4/MOD6 (Ref. 4), RELAP5/MOD1 (Ref. 5), and RELAP5/MOD2 (Refs. 6 and 7) in Fig. 6. The RELAP4/MOD6 slip model produced nonphysical oscillations in the spatial void distribution that severely altered predicted void fractions in the downstream cells. The RELAP5/MOD1 results were also oscillatory, but not nearly so severely as those of its predecessor. The new interfacial drag model implemented in RELAP5/MOD2 improved the spatial void predictions significantly with 27 axial cells in the vessel.[7] The codes RELAP5/MOD2 and

TRAC-PF1 produced a smooth and accurate prediction of the spatial void distribution.

Bottom Blowdown Test

The bottom blowdown test was simulated using TRAC-PF1 with homogeneous flow friction factors and additive loss coefficients of 0.1 and 1.0 in the break junction. As shown in Fig. 8, with an additive loss coefficient value of 0.1, TRAC overpredicted the pressure in the transient period of 20 through 30 s and underpredicted the pressure at transient times >30 s. This discrepancy between predicted and measured results may be due to the lack of sufficient spatial detail near the break to capture the exit void fraction. The TRAC predictions of the two-phase level compare favorably with the measured data, as shown in Fig. 9.

CONCLUSIONS

Predictions of two GE level swell tests were performed. The TRAC-PF1/MOD1 code results compared favorably with the measured data when appropriate time-step and grid sizes were used. Nonphysical spatial oscillations in the void fraction distribution were observed when large time steps were
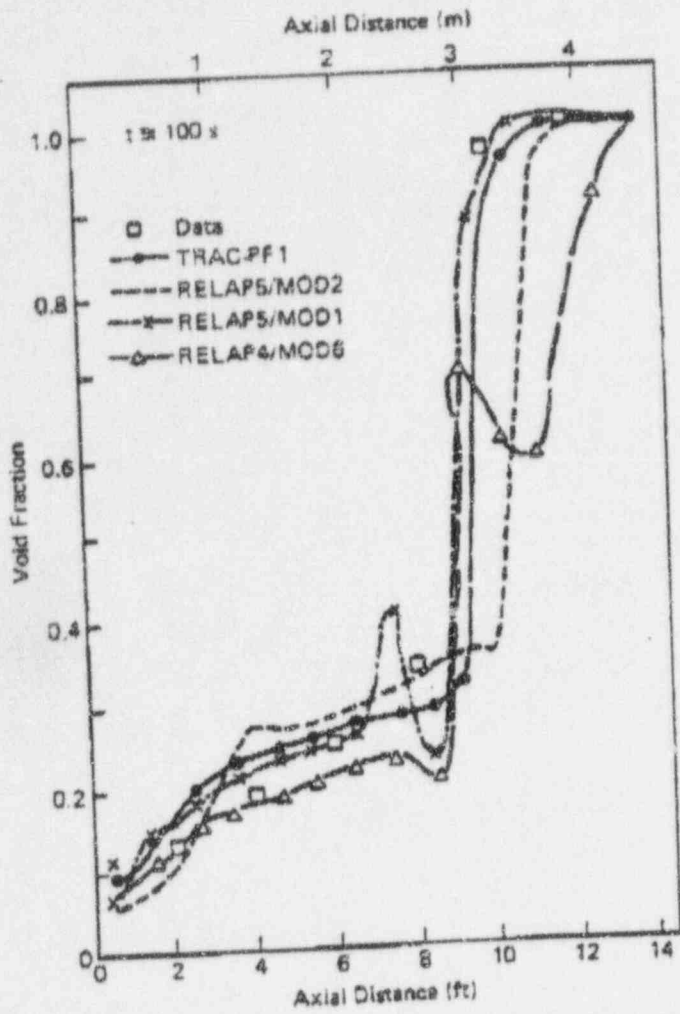
Fig. 6. Comparison between the computed void fractions using various codes and experimental data at transient time $t = 100$ s for test 1004-3.
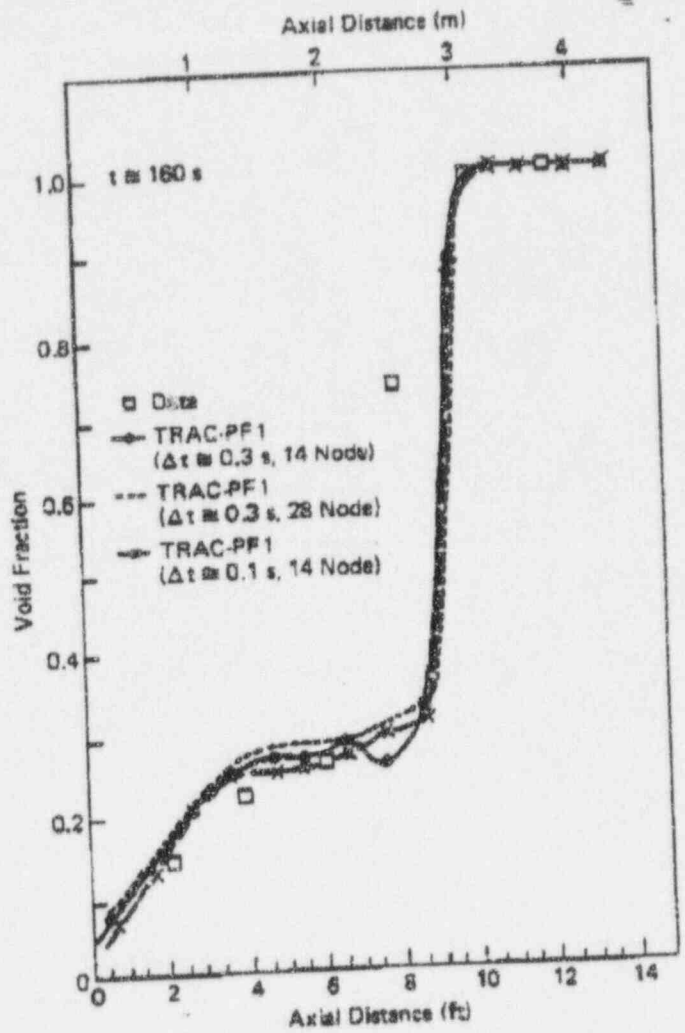
Fig. 7. Comparison between the computed and measured void fractions at transient time $t = 160$ s for test 1004-3.
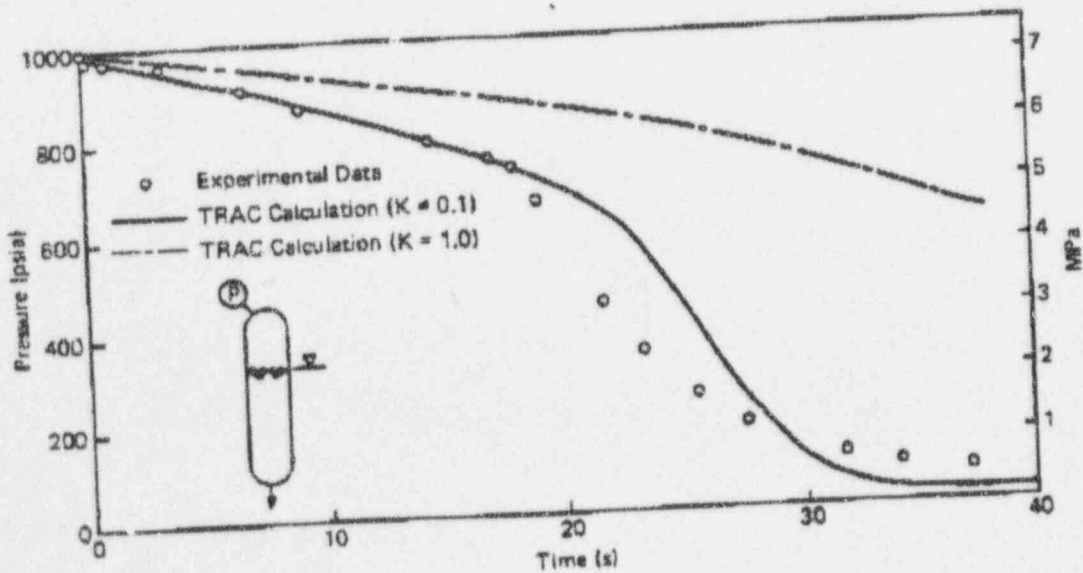

Fig. 8. Comparison of TRAC prediction of vessel pressure and experimental data for GE bottom vessel blowdown.
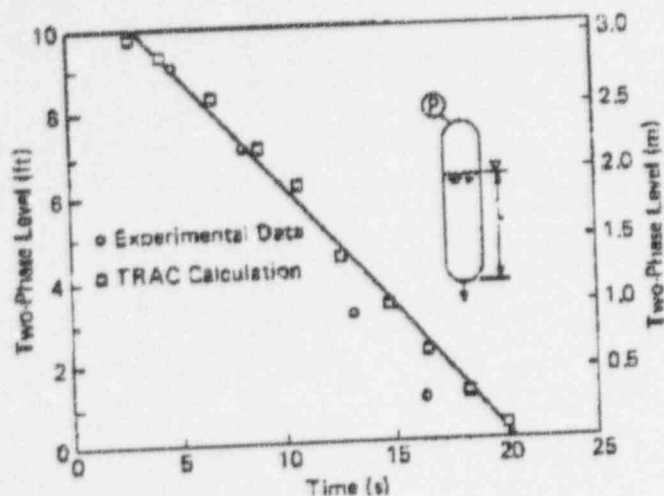
Fig. 9. Comparison of predicted two-phase level and experimental data for GE bottom vessel blowdown.

employed. These oscillations were not in evidence when a reduced time-step size was used. Reduction of the spatial grid size altered the character of the oscillations but did not eliminate them.

REFERENCES

1. "TRAC-PF1/MOD1: An Advanced Best-Estimate Computer Program for Pressurized Water Reactor Thermal-Hydraulic Analysis," Los Alamos National Laboratory (to be published).

2. J. A. FINDLAY, "BWR Refill-Reflood Program Task 4.8 — Model Qualification Task Plan," NUREG/CR-1899, U.S. Nuclear Regulatory Commission (Aug. 1981).

3. B. C. SLIFER and J. E. HENCH, "Loss of Coolant Accidents and Emergency Core Cooling Models for General Electric Boiling Water Reactors," NEDO-10329, General Electric Company (Apr. 1971).

4. "RELAP4/MOD6: A Computer Program for Transient Thermal-Hydraulic Analysis of Nuclear Reactors and Related Systems," CDAP TR 003, Idaho National Engineering Laboratory (Jan. 1978).

5. V. H. RANSOM et al., "RELAP5/MOD1 Code Manual," NUREG/CR-1826, EGG-2070, U.S. Nuclear Regulatory Commission (Nov. 1980).

6. V. H. RANSOM et al., "RELAP5/MOD2 Code Manual," EGG-SAAM-6377, EG&G Idaho, Inc. (Apr. 1984).

7. H. CHOW and V. H. RANSOM, "A Simple Interphase Drag Model for Numerical Two-Fluid Modeling of Two-Phase Flow Systems," Trans. Am. Nucl. Soc., 46, 853 (1984).

Enclosure 4

Report on Use of Full-Scale UPTF Data to Evaluate
Scaling of Downcomer and Hot Leg Two-Phase Flow Phenomena

USE OF FULL-SCALE UPTF DATA TO
EVALUATE SCALING OF DOWNCOMER (ECC BYPASS) AND HOT LEG TWO-PHASE FLOW PHENOMENA

P. S. Damerell
N. E. Ehrich
K. A. Wolfe

MPR Associates, Inc.

Abstract

The first UPTF Downcomer Separate Effects Test and the UPTF Hot Leg Separate Effects Test provide full-scale data useful for evaluating scaling effects. The downcomer test showed that subcooled ECC penetration down the downcomer at one steam flow was greater than would be predicted from several correlations using the largest available subscale data (1/5 scale by length). This is a favorable result from a licensing standpoint, i.e., actual full-scale performance is better than thought. The multidimensional flow in a large downcomer appears to be a key factor in the better delivery at large scale. The hot leg test showed that saturated water runback to the vessel in a hot leg under CCFL conditions is very close (±5%) to that predicted from the largest subscale tests (1/13 scale by area). This is an encouraging result from the standpoint of scaling. Further, this test shows there is a large margin between typical small break LOCA reflux condensation conditions and CCFL, and that the major scaled small break LOCA scaled integral facilities (PKL, Semiscale, ROSA-IV, FLECHT-SEASET) operated within the hot leg CCFL boundary, even though not necessarily at ideally scaled PWR conditions. Finally, evaluation of these data show that runback of de-entrained water in a hot leg during large break LOCA reflood is likely to occur in typical US PWRs, and the data successfully explain the observation of runback in SCTF (full-height oval hot leg) and the lack of runback in CCTF (scaled height hot leg).

Introduction

Research on the effectiveness of the emergency core cooling system (ECCS) in a pressurized water reactor (PWR) has involved a large number of separate effects and integral tests, essentially all at scaled geometry. The large number of tests have provided useful data for models and correlations of various pheonemena, and for assessment of integrated

computer codes for loss-of-coolant accident (LOCA) evaluation. One of the residual issues with regard to the accuracy of nuclear power plant calculations is the uncertainty introduced by calculating at full-scale while testing and assessing at subscale.

One of the major effects of scale is the impact of flow channel size on flow patterns and flow regimes in two-phase flow. Particularly during portions of a LOCA in which velocities are lower and gravitational forces play a much stronger role, it is known that the size of the flow section has a significant effect on the flow pattern, on the transport and retention of water in key areas, and thus on the overall course of a transient. The latter portion of a large break LOCA and a small break LOCA are examples of scenarios where gravitational (and hence size) effects are important.

Recently, separate effects tests in the Upper Plenum Test Facility (UPTF) have provided the first full-scale data on two key two-phase flow scenarios in PWR LOCA evaluation. These UPTF data provide a unique opportunity to evaluate the effect of scaling up to full-scale and to assess the scale-up capability of analytical and empirical models. Also, evaluation of these data provide improved insight and assurance about expected PWR behavior. Accordingly, it is appropriate to evaluate the data from these tests in this regard and the purpose of this paper is to describe the results of initial scaling evaluations from these tests.

The two UPTF tests discussed herein and the overall reactor safety scenarios to which they relate are as follows:

1. Downcomer Separate Effects Test -- This UPTF test investigated ECC delivery/bypass in the downcomer of a PWR. It is related to the reactor safety question of how soon and how quickly the vessel refills with ECC water at the end of the blowdown phase in a large break LOCA. The key phenomenon is the countercurrent flow limitation (CCFL) in the downcomer (i.e., downflowing water in the face of an upflowing steam/water mixture) which is strongly affected by condensation and by the multidimensionality of the downcomer. This scenario has long been considered to be scale-dependent. US licensing rules (10 CFR 50 Appendix K) artificially require no ECC delivery down the downcomer until blowdown is concluded. Scale test results from the NRC ECC Bypass Program (up to 1/5 scale by length) showed ECC does penetrate, and empirical correlations to quantify penetration were developed in that program. These correlations were generally thought to be conservative if applied to a full-scale PWR. Accordingly, this UPTF test (which was the first of four downcomer separate effects tests) helps to accurately quantify full-scale behavior.
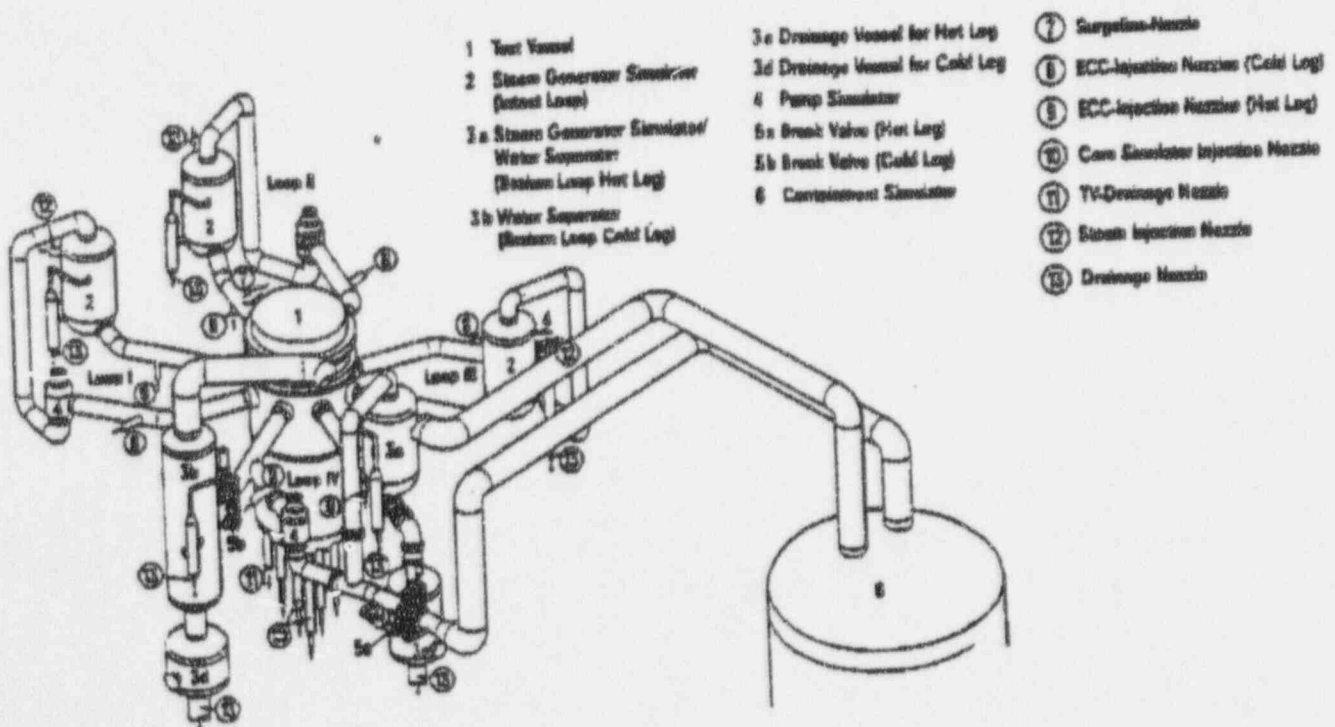
2. Hot Leg Separate Effects Test -- This UPTF test investigated steam/water countercurrent flows in the hot leg of a PWR. It is related to the reactor safety question of how readily the drain-back of water occurs in the hot legs during a small break LOCA (e.g., during reflux condensation cooling) and also to how readily de-entrained water might drain back during the reflood portion of a large break LOCA. This issue has been previously addressed with separate effects tests up to 1/13-scale (area). Accordingly, the UPTF data provide the first full-scale glimpse at this phenomenon.

This report presents brief overviews of UPTF and of the two tests (all of which have been presented elsewhere) and discusses the scaling evaluation of downcomer and hot leg phenomena.

Summary Description of UPTF

The UPTF has been previously described (References 1 and 2) and is briefly discussed here with emphasis on the downcomer and hot legs.

UPTF simulates a 4-loop German PWR which is similar to a US 4-loop Westinghouse PWR (Figure 1). A full-size reactor vessel and piping (four hot legs and four cold legs) are included in UPTF. ECC can be injected in the hot and/or cold legs of all four loops, or in the downcomer. One of the four loops contains break valves which are piped to a large containment simulator tank. The four steam generators are simulated by four steam/water separators and the four reactor coolant pumps are simulated by four passive, adjustable resistances. The reactor vessel upper plenum internals and top-of-core are full-scale replicas. The core

| 1 | Test Vessel | 3c Drainage Vessel for Hot Leg | ⑦ Surgeline-Nozzle |
2	Steam Generator Simulator (Intact Loop)	3d Drainage Vessel for Cold Leg	⑧ ECC-Injection Nozzle (Cold Leg)
3a	Steam Generator Simulator/Water Separator (Broken Loop Hot Leg)	4 Pump Simulator	⑨ ECC-Injection Nozzle (Hot Leg)
		5a Break Valve (Hot Leg)	⑩ Core Simulator Injection Nozzle
		5b Break Valve (Cold Leg)	⑪ TV-Drainage Nozzle
3b	Water Separator (Broken Loop Cold Leg)	6 Containment Simulator	⑫ Steam Injection Nozzle
			⑬ Drainage Nozzle

OVERALL VIEW OF UPTF (FROM REFERENCE 4)

FIGURE 1

is simulated by a steam/water injection system with 193 nozzles, one for each active fuel assembly which would be present in a PWR. UPTF was originally designed as an integral system test facility covering the end-of-blowdown, refill and reflood phases of a large break LOCA; as discussed in this paper it has also proven very useful as a full-scale separate effects facility covering both large and small break LOCA phenomena. UPTF can operate at up to 18 bar (260 psia) pressure and 220°C (428°F) temperature.

The UPTF vessel downcomer (Figure 2) has an inner diameter of 4.370 m (14.3 ft) and an outer diameter of 4.870 m (16.0 ft), giving a gap of 250 mm (9.8 in). The height of the downcomer from the lower edge of the downcomer skirt to the cold leg centerline is 6.64 m (21.8 ft). The four 750 mm (29.5 in) cold leg nozzles are spaced around the downcomer as shown in Figure 2. The lower plenum is 2.48 m (8.14 ft) high from vessel bottom dead-center to the lower edge of the downcomer skirt and has a volume of 24.9 m³ (880 ft³). This volume is slightly less than that of a Westinghouse PWR due to the presence of core simulator piping in the UPTF lower plenum. Table 1 compares UPTF downcomer and lower plenum configuration with that of typical Westinghouse and Combustion Engineering (CE) US PWRs*.

---

* Babcock & Wilcox (B&W) PWRs are not discussed herein because these UPTF tests are relevant mainly to Westinghouse and CE PWRs. Future UPTF tests will cover conditions relevant to B&W PWRs.
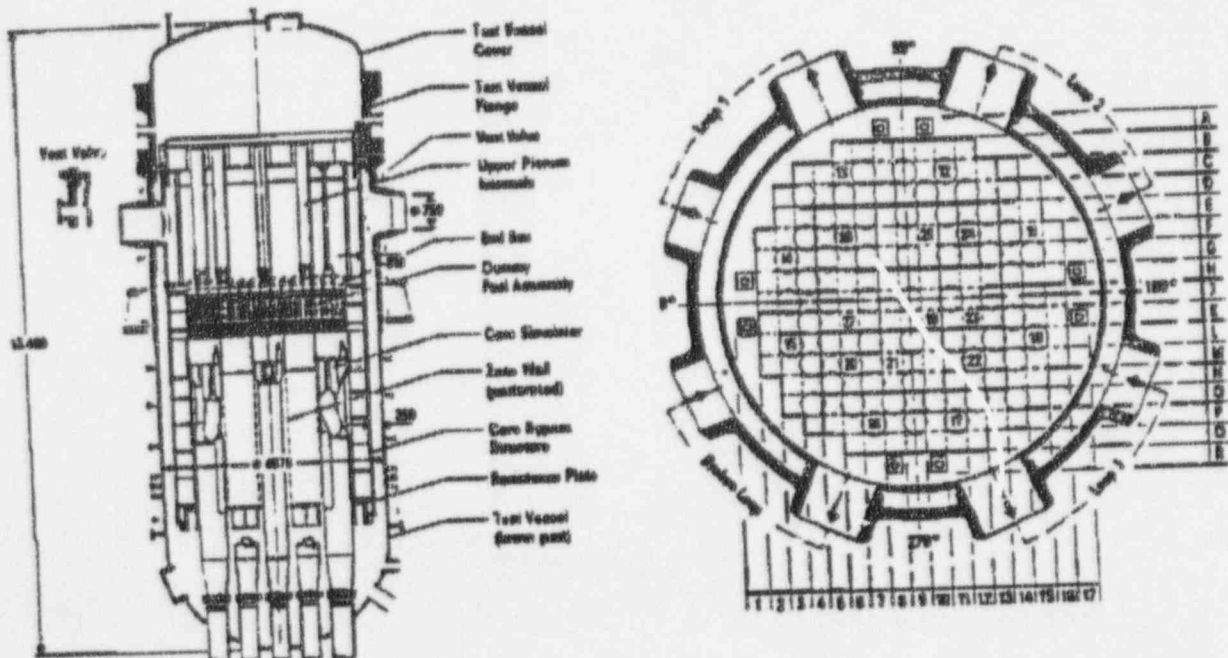
UPTF PRIMARY VESSEL (FROM REFERENCE 2)

FIGURE 2

TABLE 1

COMPARISON OF UPTF DOWNCOMER AND
LOWER PLENUM CONFIGURATION WITH TYPICAL
WESTINGHOUSE AND COMBUSTION ENGINEERING (CE) PWR'S

| Parameter	UPTF Value	Westinghouse PWR Value	CE PWR Value
Downcomer OD m (ft)	4.87 (16.0)	4.39 (14.4)	4.63 (15.2)
Downcomer Gap mm (in)	250 (9.8)	260 (10.2)	254 (10.0)
Downcomer Height, Skirt to Cold Leg Center m (ft)	6.64 (21.8)	5.33 (17.5)	6.46 (21.2)
Lower Plenum Volume m^3 (ft^3)	24.9 (880)	29.7 (1049)	22.5 (794)

Each UPTF hot leg (Figure 3) is 750 mm (29.5 in) inner diameter and has a total lateral run from the vessel to the steam generator simulator of about 8 m (26 ft). A 50° riser section rises 0.91 m (3.0 ft) at the end of the hot leg attached to the steam generator simulator. In the horizontal section of hot leg, an internal ECC injection pipe ("Hutze") is located along the bottom edge of the pipe (Figure 4). There was no injection through the Hutze in the tests discussed in this report, i.e., it is a dead space in the hot leg. The Hutze blocks an area of 0.0444 m^2 (0.478 ft^2), about 10 percent of the total pipe area. A Hutze is present in German PWRs but not in US PWRs. Table 2 compares UPTF hot leg configuration with that of typical Westinghouse and CE US PWRs.

TABLE 2

COMPARISON OF UPTF HOT LEG CONFIGURATION WITH TYPICAL
WESTINGHOUSE AND COMBUSTION ENGINEERING (CE) PWR'S

Parameter	UPTF Value	Westinghouse PWR Value	CE PWR Value
Diameter, m (in)	0.750 (29.5)	0.737 (29)	1.07 (42)
Hydraulic Diameter, m (in)	0.639 (25.2)	0.737 (29)	1.07 (42)
Flow Area, m^2 (ft^2)	0.397 (4.28)*	0.427 (4.59)	0.894 (9.62)

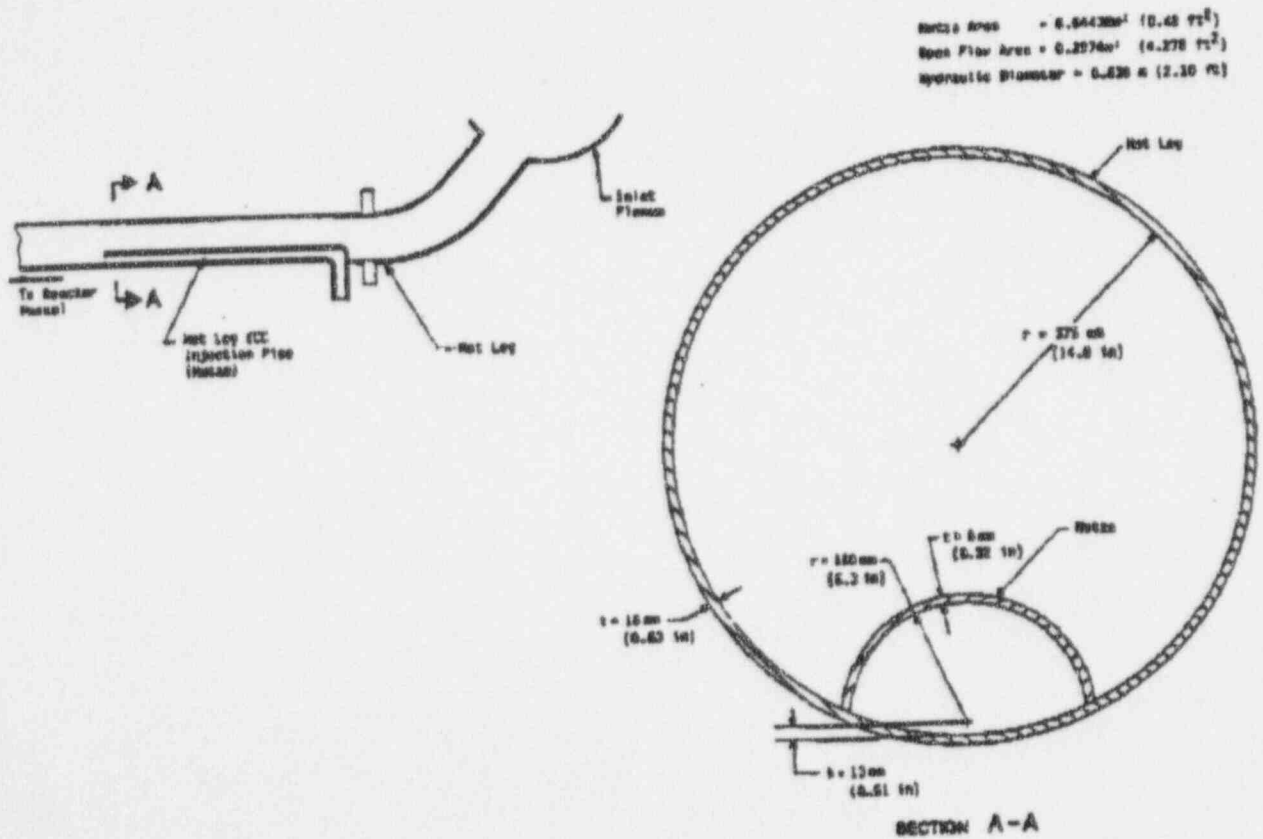* 0.4418 m^2 within diameter minus 0.0444 m^2 blocked by "Hutze".
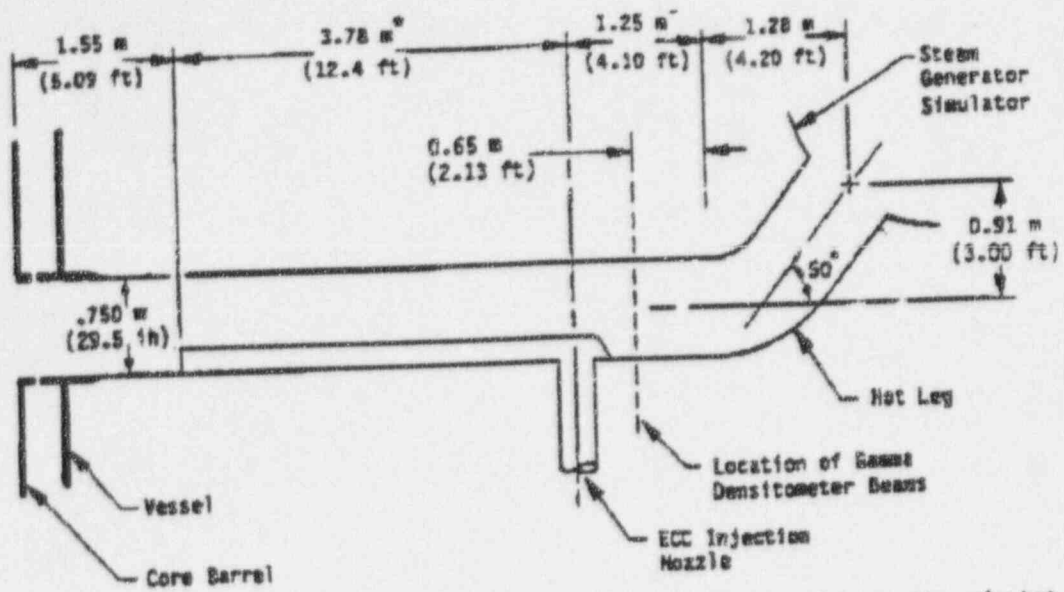
* Note: These dimensions are for the UPTF broken loop hot leg, which was the only hot leg used in the Hot Leg Separate Effects Test. In the intact loops, these two dimensions are slightly larger (3.86 m and 1.34 m).

UPTF HOT LEG CONFIGURATION

FIGURE 3

CONFIGURATION OF INTERNAL ECC INJECTION
PIPE (HUTZE) IN UPTF HOT LEG

FIGURE 4

148

Overview of UPTF Downcomer Separate Effects Test

The test conditions and results from the first UPTF Downcomer Separate Effects test are described elsewhere (Reference 3) and are briefly reviewed here. The test was run in two phases: transient and steady. In both phases the loops were blocked at the pump simulators, and the cold leg break valve was used to allow flow to discharge from the system. Also in both phases, 30°C (86°F) ECC was injected into the three intact cold legs at a rate of 500 kg/sec/loop (1100 lb/sec/loop). A small amount of nitrogen (about 0.15 kg/sec/loop or 0.33 lb/sec/loop) was injected with the ECC to simulate the nitrogen coming out of solution in a PWR accumulator.

In the transient phase, the facility was initialized at 18 bar (260 psia) with the cold leg break valve closed and the containment at 2.5 bar (37 psia). The lower plenum was approximately half full of saturated water. The test was initiated by starting ECC flow to the cold legs and opening the break valve to full-open at about the same time. This produced a depressurization transient with steam (from expansion and flashing) and entrained water escaping up the downcomer and out the break, and subcooled ECC water entering the top of the downcomer from the three intact legs (Figure 5). The transient lasted about 25 seconds.
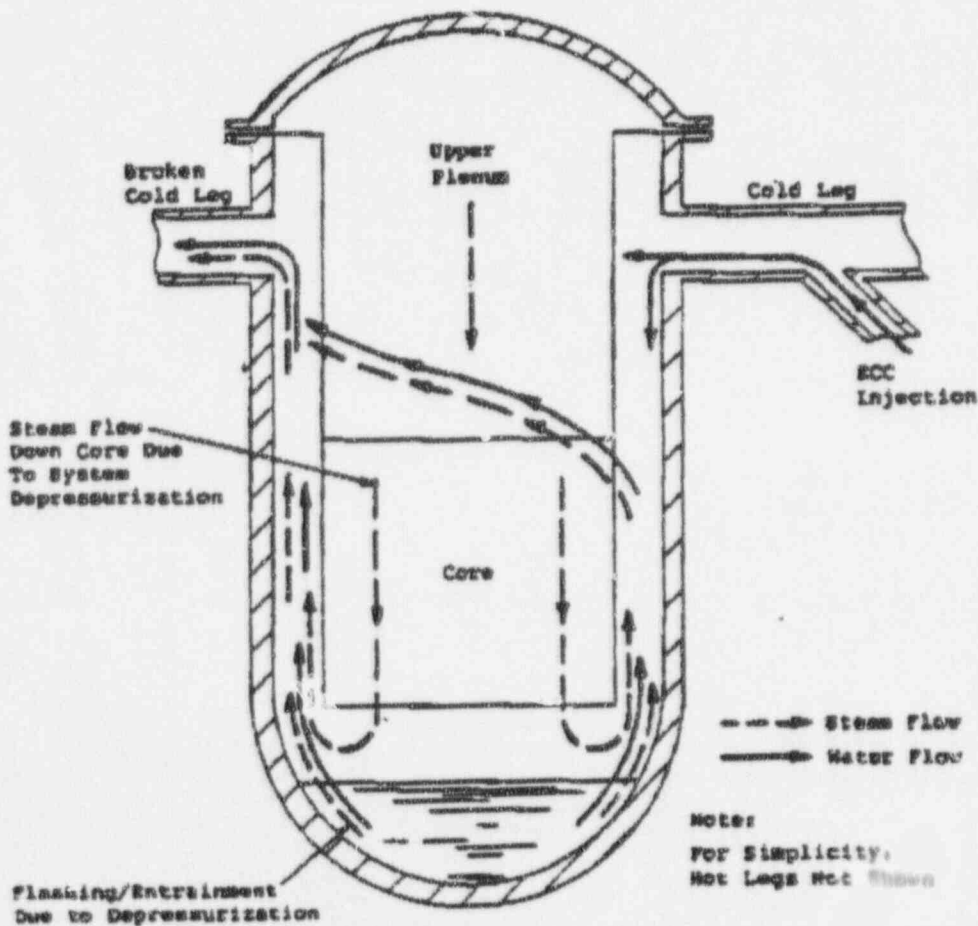

DIAGRAM OF FLOW CONDITIONS DURING TRANSIENT PHASE
OF UPTF DOWNCOMER SEPARATE EFFECTS TEST

FIGURE 5

In the steady phase, the facility and containment were initialized at 2.5 bar (37 psia) with the cold leg break valve fully open. There was a small initial saturated water inventory in the lower plenum. To start the test, a preprogrammed steam flow of about 320 kg/sec (705 lbm/sec) was injected in the core which flowed to the lower plenum, up the downcomer and out the break. After a few seconds, ECC injection in the cold legs was initiated (Figure 6). The downcomer test was over in about 20 seconds at which time the lower plenum filled to nearly the bottom of the core.

As discussed in Reference 3, the transient phase showed a mixture of ECC bypass (out the break) and delivery down the downcomer. At the conclusion of the blowdown the lower plenum was nearly full, i.e., the inventory increased during the transient. Local downcomer measurements showed a strong asymmetry in the flow, with ECC delivery preferentially occuring on the side of the downcomer away from the break. The steady phase showed nearly complete penetration (about 80 percent) of ECC down the downcomer against the upward steam flow. Once again, local downcomer measurements showed strongly asymmetric flow with ECC penetration favoring the side of the downcomer away from the break.
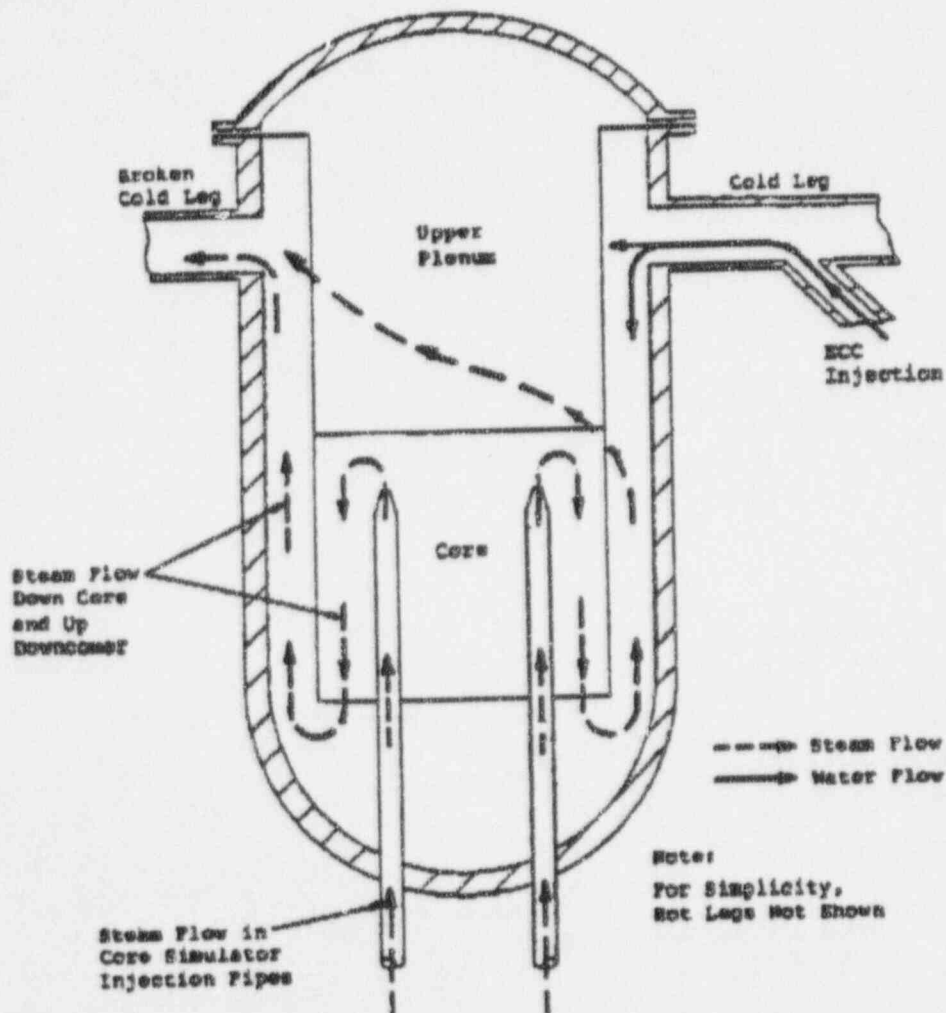

DIAGRAM OF FLOW CONDITIONS DURING PSEUDO—STEADY
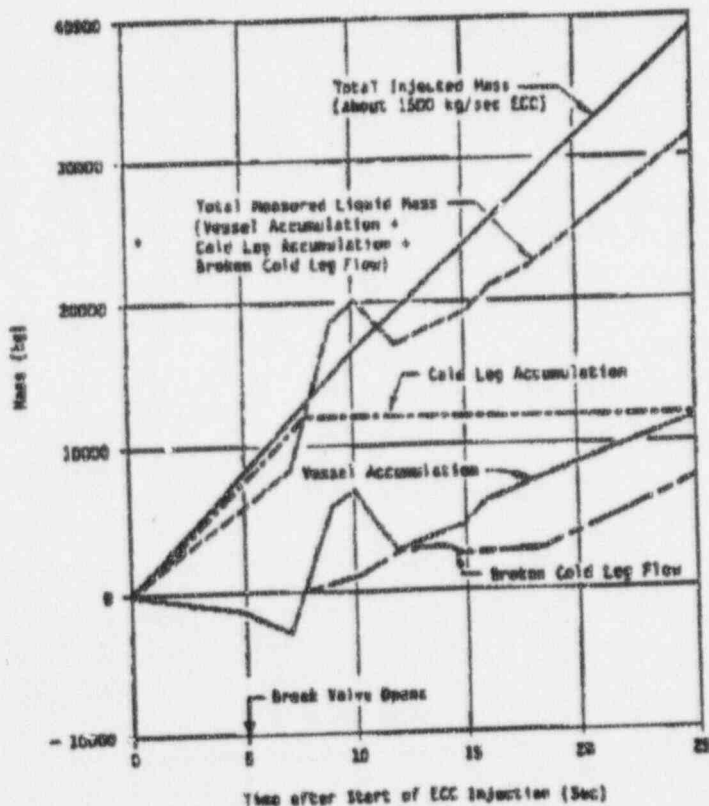PHASE OF UPTF DOWNCOMER SEPARATE EFFECTS TEST

FIGURE 6

Evaluation of ECC Delivery/Bypass Scaling

To best quantify the results of the UPTF downcomer separate effects test for evaluation of scaling, mass balances were performed for each test phase. The results of the mass balance are shown in Figure 7 for the transient phase and in Figure 8 for the steady phase.

Figure 7 shows that when the transient started there was a period during which ECC was stored in the intact cold legs. This storage was inferred from thermocouple rakes in one cold leg which showed subcooling appearing at all locations over this time frame. There were no direct measurements of the amount of mass stored; the curve shown assumes the closed end pipes filled according to the injection rate. Vessel inventory decreased slightly while the legs were filling due to flashing.

When the cold legs filled and water was being delivered to the downcomer, vessel inventory rapidly increased, indicating ECC delivery. Small indications of bypass out the broken cold leg first appeared at this time as well. Over a period of about 15 seconds, delivery and bypass both occurred. The "spike" in delivery is apparently attributable to a brief emptying of the cold leg inventory -- a corresponding decrease does not appear in the cold leg curve because cold leg inventory was inferred rather than measured, as discussed above. At the end of the depressurization (about 25 seconds), the lower plenum was essentially full and less than half the injected water had been bypassed out the broken cold leg.

UPTF DOWNCOMER SEPARATE EFFECTS TEST
MASS BALANCE FOR TRANSIENT PHASE

FIGURE 7

Figure 8 shows that during the steady test there was also an initial period during which the cold legs filled, followed by substantial delivery to the vessel with limited bypass out the broken cold leg. At approximately 20 seconds after the start of ECC injection, the lower plenum was essentially full, and only 20 percent of the ECC had been bypassed out the broken cold leg.

The evaluation of scaling using the UPTF test results was found to be most useful using the steady phase test results; accordingly, they are discussed first below. Figure 9 shows a downcomer dimensionless flow plot using the parameters j_g^* and j_f^* where

$$j_g^* = M_g (\rho_g)^{1/2} / \rho_g A ((\rho_f - \rho_g) gW)^{1/2}$$

$$j_f^* = M_f (\rho_f)^{1/2} / \rho_f A ((\rho_f - \rho_g) gW)^{1/2}$$

where   M = mass flow rate of gas or liquid

                A = downcomer area (3.62 m^2 or 39 ft^2 for UPTF)

                ρ = density of gas or liquid

                g = gravity

                W = downcomer circumference (14.5 m or 47.6 ft for UPTF)
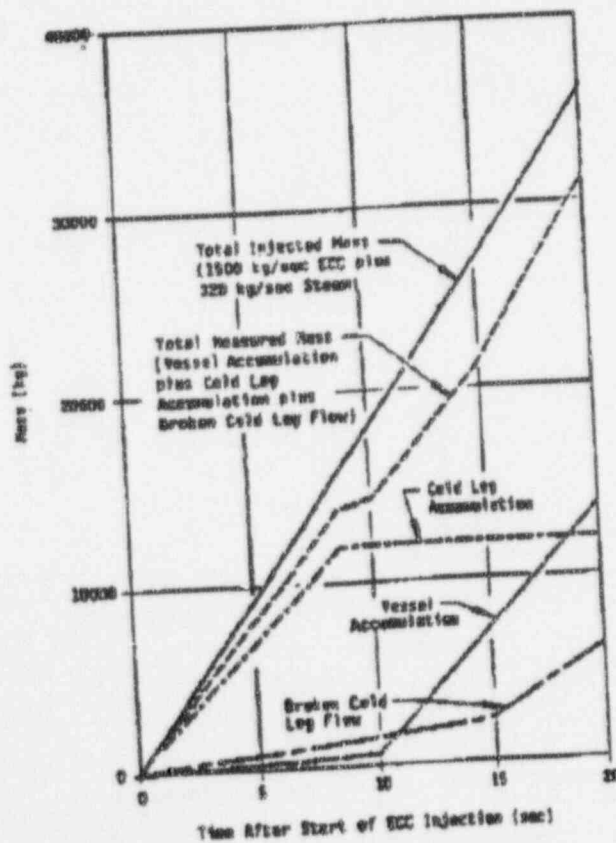
UPTF DOWNCOMER SEPARATE EFFECTS TEST
MASS BALANCE FOR STEADY PHASE
FIGURE 8

152

Correlation 1: $(j_g^* - F\, j_{g,}^*\, T_{cond})^{1/2} + M\, j_f^{*\,1/2} = C$

Correlation 2: $j_g^{*\,1/2} - F\, j_{g,}^*\, T_{cond}^{1/2} + M\, j_f^{*\,1/2} = C$

$$j_g^* = \frac{\dot{M}_g}{\rho_g A}\sqrt{\frac{\rho_g}{\Delta\rho g W}} \qquad j_f^* = \frac{\dot{M}_f}{\rho_f A}\sqrt{\frac{\rho_f}{\Delta\rho g W}} \qquad j_g^*,\, T_{cond} = j_{f,in}^* \frac{C_p\,(T_{sat} - T_\ell)}{h_{fg}}\sqrt{\frac{\rho_f}{\rho_g}}$$

Parameter	Momentum Flux Scaling		j^* Scaling	
	Correlation 1	Correlation 2	Correlation 1	Correlation 2
F	0.281	0.209	0.281	0.209
M	0.896	0.822	0.896	0.822
C	0.250	0.230	0.369	0.344
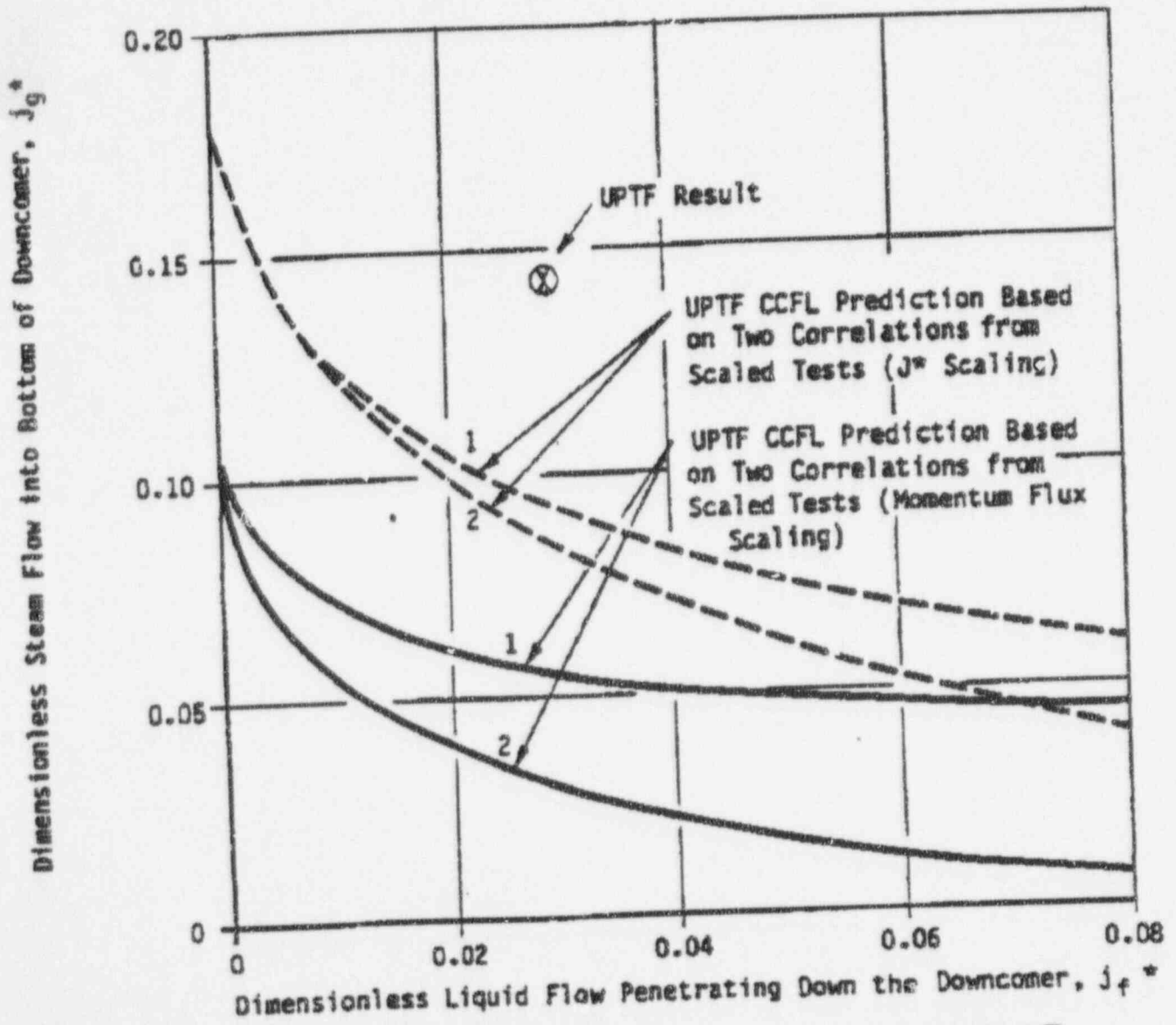
COMPARISON OF UPTF DOWNCOMER TEST RESULT
WITH PREDICTIONS BASED ON 1/5 SCALE TESTS

FIGURE 9

From previous scaled tests in the NRC ECC Bypass Program (References 4 - 8), j* correlations were developed using data from 1/30, 1/15, 2/15 and 1/5 scale (by length). A convenient summary of the correlations is in Reference 4.

The curves shown on Figure 9 represent the CCFL boundary calculated for UPTF based on the largest scale data available from the previous scaled tests (1/5-scale). The four lines show four possible approaches for calculating the UPTF boundary: the two lower curves represent a "constant momentum flux" scaling approach with two different forms of correlating the 1/5-scale data; and the two upper curves represent a "constant j*" scaling approach with two different forms of correlating the 1/5-scale data. The two correlation forms (labeled 1 and 2 on Figure 9) each correlated some of the subscale data more favorably -- there is no clear basis for recommending one over the other. The lower curves are the NRC-recommended approach for downcomer CCFL based on the scaled tests in the NRC ECC Bypass Program. The upper curves represented a more "realistic" approach which was not recommended by the NRC because it could not be demonstrated to be conservative at full-scale based on the scaled tests. The main result of the UPTF downcomer separate effects test is that the full-scale test shows more ECC penetration than would be predicted by either the NRC-recommended or realistic approaches at full-scale. Hence, there appears to be a beneficial effect of large scale, which may be related to improved condensation, to large channel hydraulics, or to both. The observation of the strong asymmetry in the downcomer, i.e., preferential ECC downflow on the side away from the break (see Reference 3), indicates that the large channel effect is probably significant.

The main result of the transient phase of the downcomer separate effects test is that it showed that ECC penetrates the downcomer and refills the lower plenum even while the primary system is continuing to depressurize. Although scaled tests suggested this would occur, this full-scale test provides the best direct evidence. The UPTF test was reasonably PWR-typical with regard to lower plenum inventory and ECC subcooling. The ECC injection rate was somewhat low and the depressurization somewhat prolonged in comparison to a typical PWR LOCA, but these differences do not affect the validity of the overall result discussed above. The main use of the transient case is as a full-scale benchmark analysis case for computer codes.

It is not feasible to run in UPTF a direct counterpart transient test to previous scaled ECC bypass tests, due to some particular choices (non-PWR-typical) made in plenum volume and containment pressure in the previous scaled facilities. Accordingly, future downcomer separate effects tests will focus on steady-state downcomer CCFL conditions, in an attempt to further evaluate scaling by comparing UPTF results with CCFL curves derived from previous scaled tests.
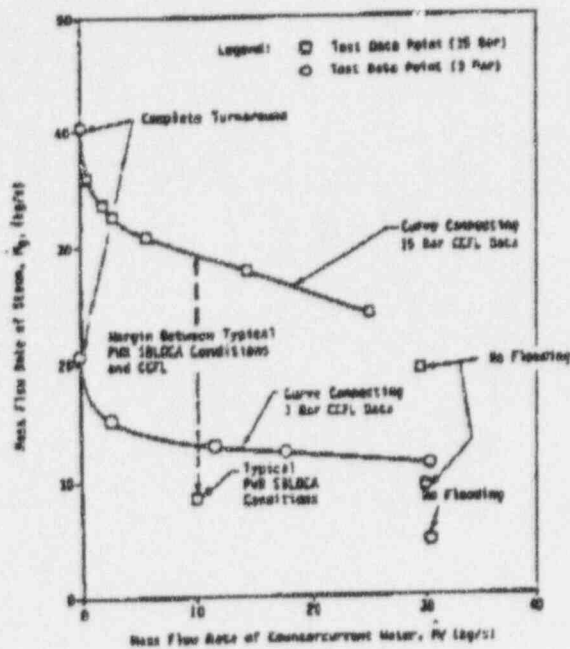
Overview of the Hot Leg Separate Effects Test

The test conditions and results from the UPTF Hot Leg Separate Effects Test are described elsewhere (Reference 9) and are briefly reviewed here. The test was run using only the broken loop hot leg of the UPTF. The test was performed as several steady phases, each consisting of steam injection into the primary vessel which flowed out the broken loop hot leg, and saturated water injection in the steam generator simulator plenum which could either flow back down the hot leg toward the vessel or out of the system through the steam generator simulator (Figure 10). Six separate steady flows were obtained at 3 bar (44 psia) system pressure and 10 flows were obtained at 15 bar (218 psia) system pressure. In all cases water flow was established prior to steam flow. The intent of obtaining several flows at each pressure was to "map out" the CCFL boundary. Also, one of the flows at 15 bar simulated conditions in a Westinghouse 4-loop PWR during the reflux condensation mode, which can occur during an SBLOCA.
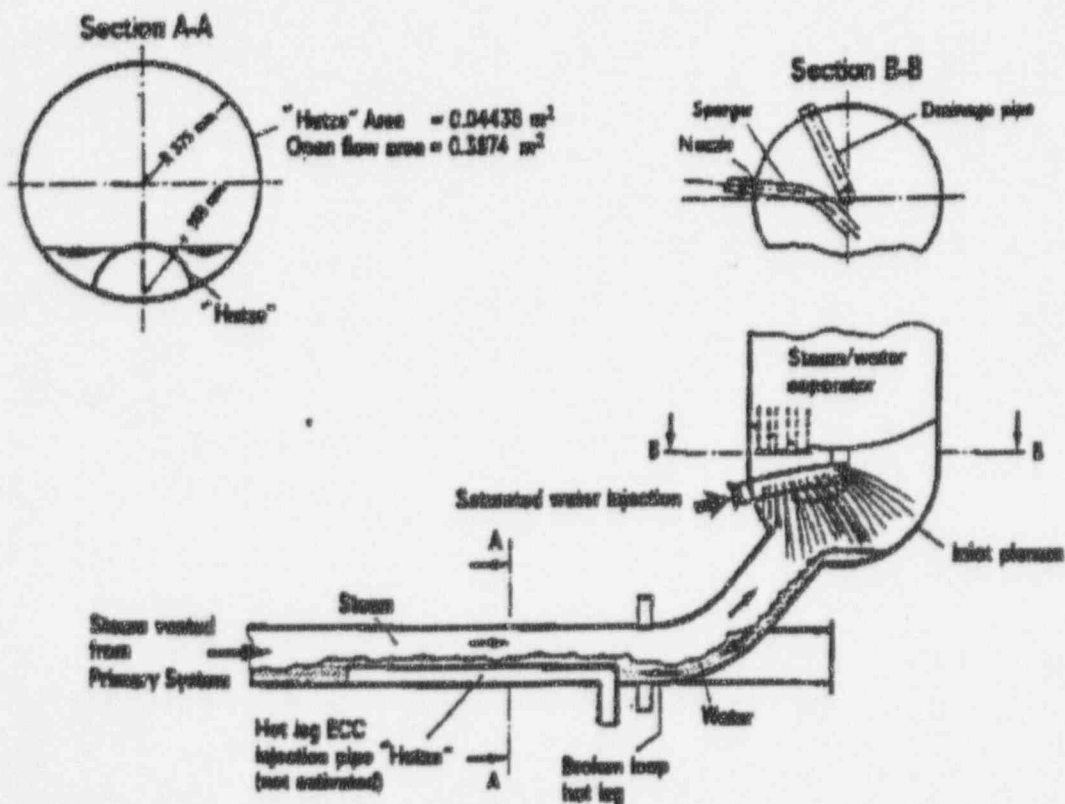
UPTF HOT LEG SEPARATE EFFECTS TEST
OVERALL FLOW CONDITIONS
(FROM REFERENCE 4)

FIGURE 10

UPTF HOT LEG SEPARATE EFFECTS TEST
SUMMARY OF DATA

FIGURE 11

Figure 11 shows the measured flows at the two test pressures, and Figure 12 shows the data on a dimensionless j* plot, where

$$j_g^* = M_g \, (\rho_g)^{1/2} / \rho_g A \, ((\rho_f - \rho_g) \, g D_h)^{1/2}$$

$$j_f^* = M_f \, (\rho_f)^{1/2} / \rho_f A \, ((\rho_f - \rho_g) \, g D_h)^{1/2}$$

The variables are as defined previously and D_h is the hydraulic diameter, which is .639 m (2.10 ft) for the UPTF hot leg at the "Hutze".
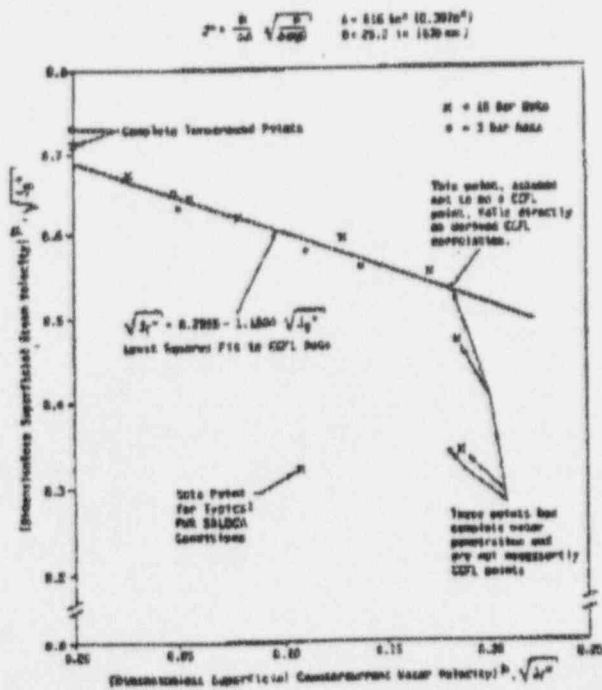
UPTF HOT LEG SEPARATE EFFECTS TEST
RESULTS SHOWN ON J* PLOT

FIGURE 12

On the j* plot, the 3 bar (44 psia) and 15 bar (218 psia) data correlate favorably. The line drawn through the data on Figure 12 is the "best-fit" experimental correlation to the UPTF data.

The results of this test provided direct demonstration that there is significant margin against hot leg CCFL during the reflux condensation phase of an SBLOCA. This is shown in Figure 12 by the fact that the "typical" point is substantially below the CCFL boundary. This point was chosen based on conservative assumptions such as relatively high power and one steam generator inactive, etc. Accordingly, this result provides direct and convincing evidence that substantial margin exists.
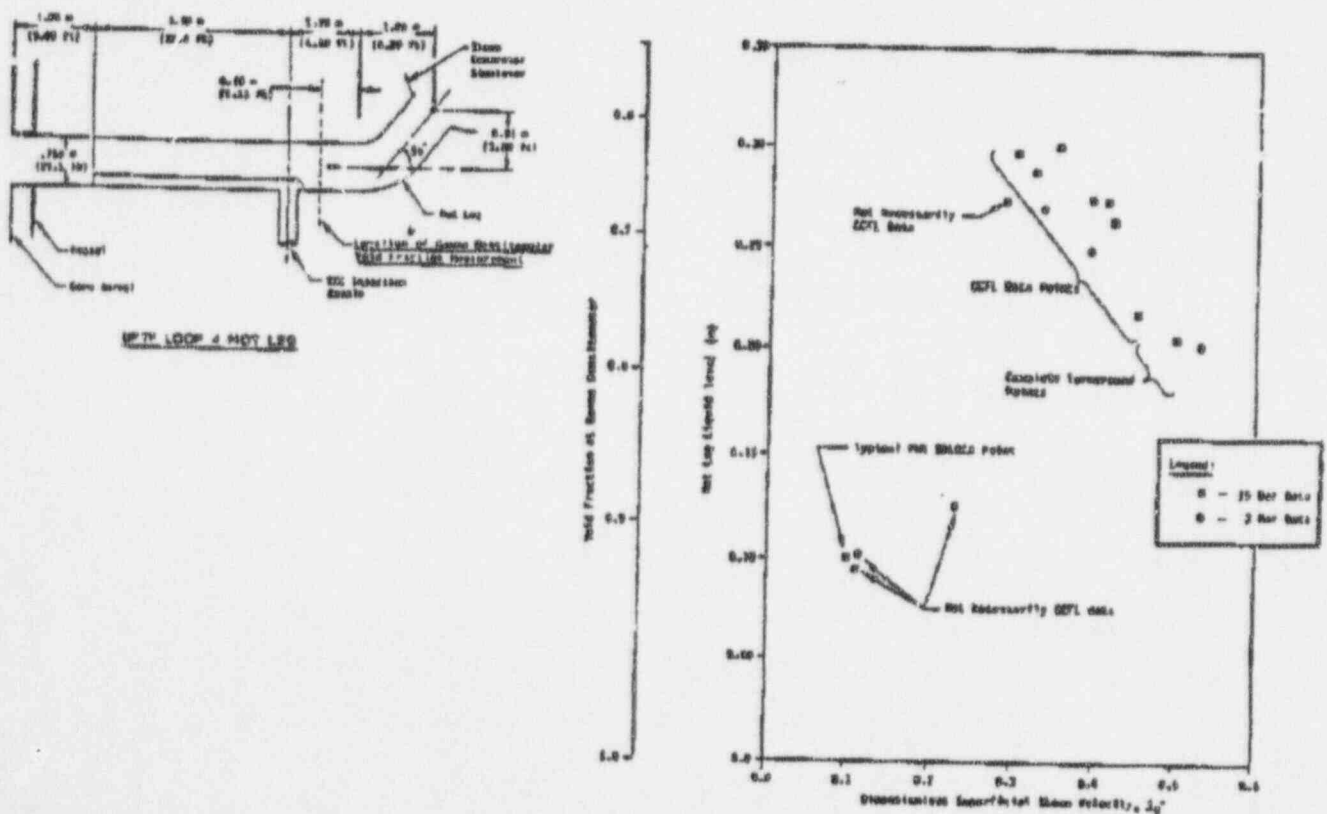
Figure 13 shows the measured hot leg level and void fraction for all of the tests, plotted against j_g^*, the dimensionless gas flow. These data are from a three-beam gamma densitometer located just on the vessel side of the hot leg riser bend, as shown on the figure. There is no "Hutze" obstructing the bottom of the hot leg in this short section of hot leg. The data clearly indicated a stratified regime and show significant water presence in this region of the hot leg. These data appear to show that CCFL is being controlled by the hot leg (i.e., CCFL is not occurring in the riser or steam generator simulator), since water is not absent from the hot leg when there is zero net penetration to the vessel.

UPTF HOT LEG SEPARATE EFFECTS TEST
MEASURED HOT LEG LEVEL AND VOID FRACTION AS
A FUNCTION OF DIMENSIONLESS STEAM VELOCITY

FIGURE 13

Evaluation of Hot Leg CCFL Scaling

Several theoretical and scaled, separate effects studies of hot leg CCFL or generalized horizontal channel CCFL have been carried out, including:

- Richter, et al (Reference 10) -- 1/13 scale by area compared to Westinghouse PWR

- Gardner (Reference 11) -- Theoretical

- Wallis (Reference 12) -- .0254 m (1-inch) square channel (approx. 1/660 scale by area compared to Westinghouse PWR)

- Ohnuki (Reference 13) -- 1/840 scale to 1/93 scale by area compared to Westinghouse PWR

- Krolewski (Reference 14) -- 1/210 scale by area compared to Westinghouse PWR

Also, Transient Reactor Analysis Code (TRAC) predictions of the UPTF test were performed. Each of these previous studies provides a way to predict full-scale hot leg CCFL behavior. In all cases, j^* is the key parameter in scaling.

Figure 14 shows the UPTF data compared to the full-scale predictions based on five of the six studies mentioned above, on a j^* plot. In the
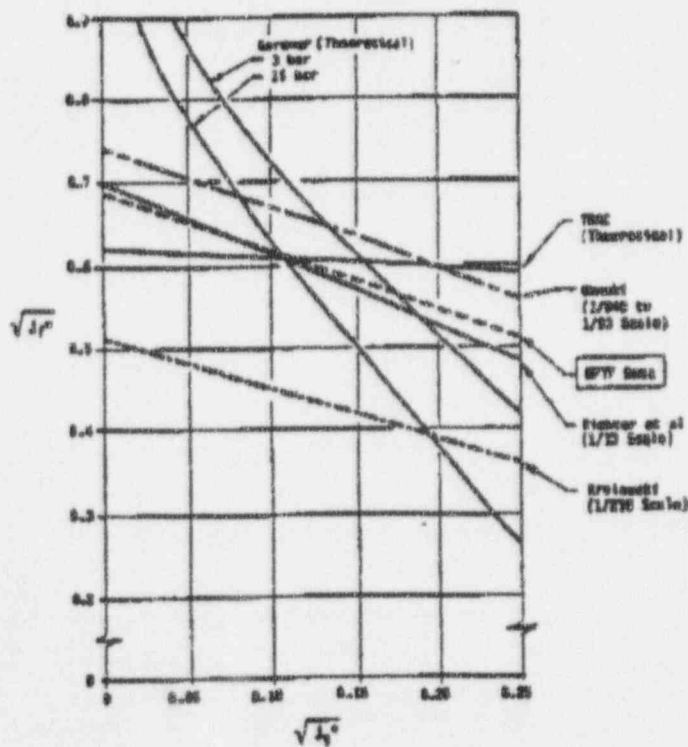
UPTF HOT LEG SEPARATE EFFECTS TEST
COMPARISON OF DATA TO THEORETICAL MODELS AND CORRELATIONS
FROM SMALL SCALE TESTS

FIGURE 14

158

UPTF HOT LEG SEPARATE EFFECTS TEST
COMPARISON OF UPTF HOT LEG VOID FRACTIONS TO
WALLIS CORRELATION

FIGURE 15

case of the Wallis correlation, which is a j*/void fraction correlation, the comparison is on Figure 15. The results of the comparisons shown on Figures 14 and 15 are as follows:

- Very close agreement is obtained between the UPTF data and the Richter, et al correlation, which is the largest subscale data previously available. The agreement is ±5 percent. This agreement confirms that the j* correlation approach appears to be valid. The close comparison indicates that scaling up across an order of magnitude (based on pipe area) is successful and is therefore an encouraging result.

- Close agreement is obtained between the UPTF data and the Wallis correlation which is based on void fraction rather than liquid flow. This indicates that the basic approach of this correlation (once again, a j* correlation) appears correct for scaling, but that implementing this model to calculate liquid flows is dependent on knowing an accurate void fraction.

- Significant deviation is observed in the case of the Ohnuki and Krolewski correlations. This is considered to be due to the small scale of the underlying tests and the strong effect of the riser bend in the previous tests. The Ohnuki tests, for example, showed that changes in the geometry of the riser section (e.g., length and angle) could significantly affect the flooding. It is not known if this sensitivity is PWR-typical; this makes it difficult to "scale-up" these small-scale results.

- The predictions using the Gardner theoretical model do not agree favorably with the UPTF data. The flooding mechanism presumed in the model (i.e., unstable stationary disturbance) does not appear to realistically reflect the true flow behavior in a PWR hot leg.

- The predictions from TRAC show a nearly "bi-stable" behavior with changing gas flow rather than the gradual CCFL boundary. The reasons are still being investigated.

Overall, the comparison with previous theoretical and scaled results is very favorable in that the results from simulated hot leg separate effects tests with one order of magnitude lower area were sufficient to accurately predict full-scale behavior.

In addition to these separate effects comparisons discussed above, several PWR integral tests of small and large break LOCAs have been conducted. In the small break case, these facilities demonstrated reflux condensation occurs without apparent hold-up due to hot leg CCFL. The major small break facilities investigating reflux condensation are:

- Semiscale (References 15 and 16) -- 1/1705 scale

- FLECHT-SEASET (Reference 17) -- 1/307 scale

- PKL (References 18 and 19) -- 1/134 scale

- ROSA-IV LSTF (Reference 20) -- 1/48 scale

The conditions achieved in reflux condensation tests in the four subscale SBLOCA facilities are plotted on a j* graph along with the correlation of UPTF results in Figure 16. Also shown in this figure is a band of "PWR conditions" which roughly envelope SBLOCA reflux condensation conditions. This figure shows that although the scaled facility conditions tend to be scattered about the graph, they are all well within the CCFL boundary, as are the PWR conditions. The PKL points, which deviate most from PWR conditions, tend to be a result of the hot leg area scaling used in these tests, which did not seek to preserve j* as in the other tests. The major conclusions, though, are that for all of the
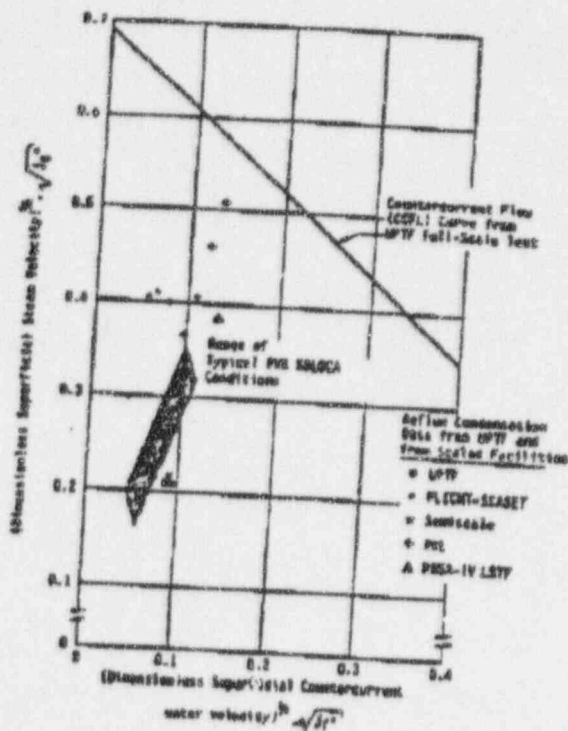
COMPARISON OF SMALL-SCALE FACILITY
REFLUX CONDENSATION EXPERIMENTAL CONDITIONS
TO UPTF TEST RESULTS

FIGURE 20

facilities, the observation of reflux condensation without hold-up from hot leg CCFL is consistent with the UPTF data, and that the scale facilities did not distort PWR hot leg behavior in a major phenomenological way.

The reflux condensation results are applied to US PWR's on Figure 17. This figure shows hot leg CCFL curves calculated for the most limiting Westinghouse and CE plants (3800 MW(t) in both cases) at 80 bar (1160 psia). Also shown are conservatively calculated SBLOCA reflux condensation conditions for both plants. The large margin is evident in both cases.

In the large break case, hot leg CCFL is only an important consideration during the reflood phase of the transient. The major, large scale reflood facilities which allow a detailed evaluation of hot leg effects are:

-    Cylindrical Core Test Facility (CCTF) -- 1/21 scale

-   Slab Core Test Facility (SCTF) -- 1/21 scale with full-height hot leg
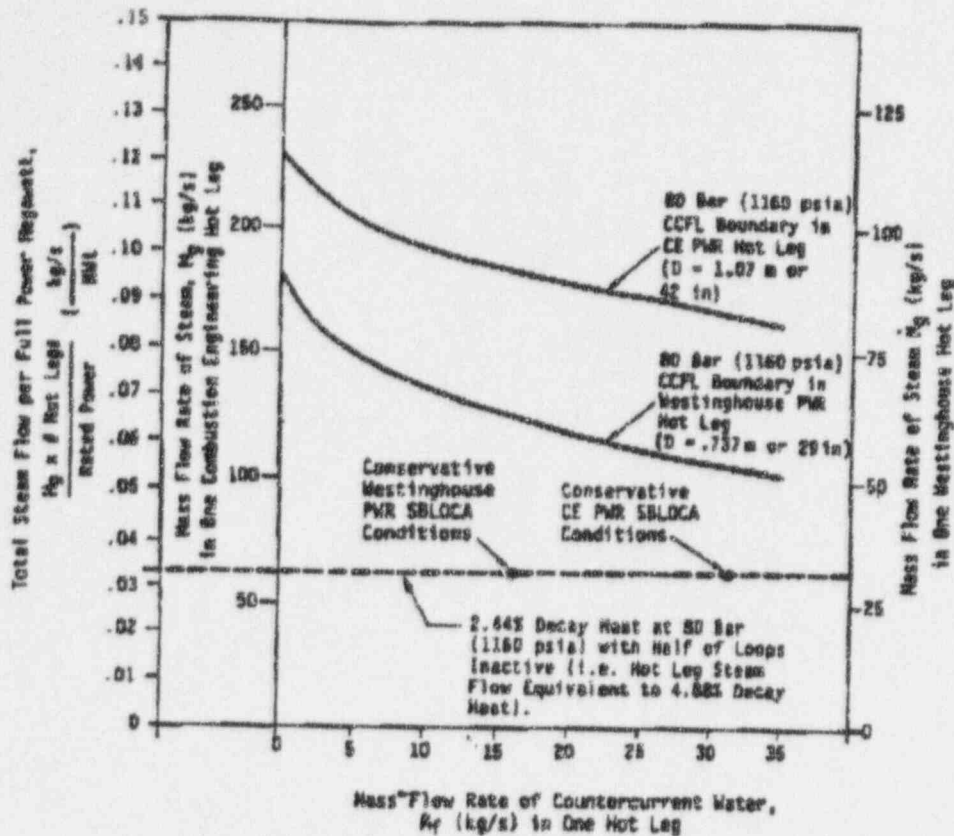
PREDICTED HOT LEG CCFL BEHAVIOR IN U.S. PWRs
COMPARED WITH SBLOCA REFLUX CONDENSATION
FLOW CONDITIONS

FIGURE 17

In CCTF, no evidence of counterflowing water during reflood was observed, i.e., any water reaching the hot legs tended to be swept through the primary coolant loops by the steam flow. In SCTF, though, hot leg water runback to the vessel by countercurrent flow was observed and directly measured. It is noted that due to the unique cross-section of the SCTF hot leg (oval) there may have been greater de-entrainment and more water available for runback in the hot leg.

The conditions achieved in the CCTF and SCTF large break reflood tests are indicated on a j^* graph along with the correlation of UPTF results in Figure 18. The steam flow j_g^* associated with typical PWR reflood conditions is also shown on this graph. As indicated on the graph, counterflowing water during reflood would be expected in SCTF but not in CCTF, i.e., consistent with observations. The CCTF/SCTF difference is due to the height of the hot leg (full-scale in SCTF but not in CCTF). The figure shows the SCTF results, in this regard, are closer to PWR-typical. As Figure 18 shows, counterflowing water would be expected in both Westinghouse and CE PWR's.

162
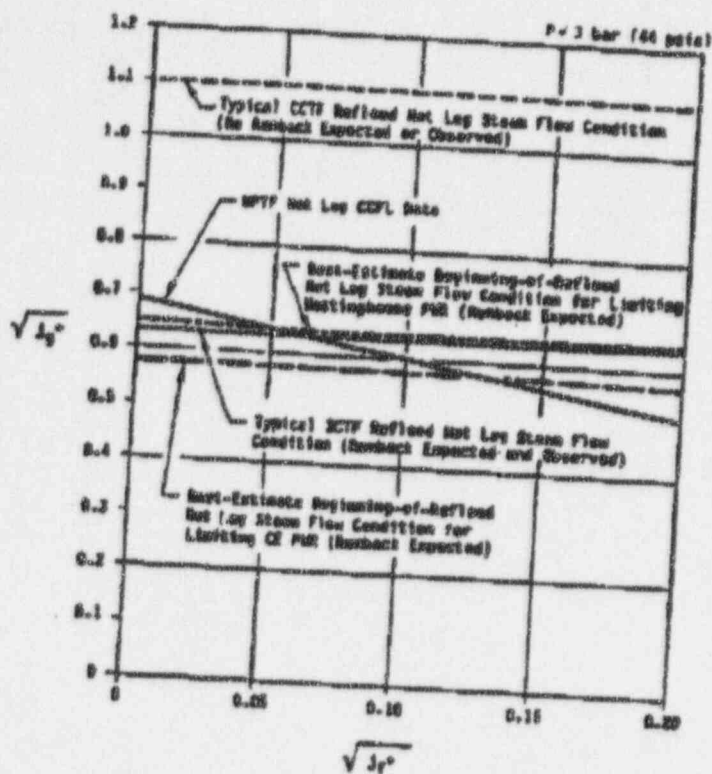
EVALUATION OF HOT LEG RUNBACK
DURING LARGE BREAK LOCA REFLOOD IN CCTF, SCTF
AND A PWR BASED ON UPTF HOT LEG TEST RESULTS

FIGURE 18

Conclusion

The UTPF Downcomer Separate Effects Test and Hot Leg Separate Effects Test have provided useful information for evaluation of scaling. For both tests the direct results convey favorable and encouraging conclusions, i.e., water penetrates to the reactor vessel through a downcomer or a hot leg as well as or better than would be predicted from subscale results. For the downcomer situation, the present test data do not provide a broad enough base to evaluate the accuracy of scaling CCFL up from previous tests. The UPTF results presently available though, do suggest that j* scaling from previous scales provides at least a conservative approach, and that determination of a precise realistic approach will have to await upcoming UPTF test results. In the hot leg, the UPTF data show that predictions from the largest subscale tests (Richter, et al at 1/13 scale based on area) are quite accurate (±5 percent). The correlation which gives this successful scaling is based on the j* parameter, indicating it appears to be the correct approach. Application of the UPTF hot leg results to US PWR's indicates that: (1) during SBLOCA reflux condensation, there is a significant margin between actual flows and the CCFL boundary, as expected; and (2) during large break LOCA reflood runback is likely for water de-entrained in the hot legs.

163

References

1.   Hofmann, K., "Status of the German UPTF Program," presented at the
     13th Water Reactor Safety Information Meeting, October 22 - 25,
     1985.

2.   Weiss, P., Sawitzki M. and Winkler, F.; "UPTF, a Full-Scale PWR
     Loss-of-Coolant Accident Program," Atomkern-Energie Kerntechnik,
     Vol.49, 1986.

3.   Hertlein, R. and Weiss, P.; "UPTF Experiment: PWR ECC Downcomer
     Countercurrent Flow Under Steam and Two-Phase Upflow Condition,"
     presented at the 15th Water Reactor Safety Information Meeting,
     October 26 - 29, 1987.

4.   "1/5-Scale Countercurrent Flow Data Presentation and Discussion,"
     NUREG/CR-2106, November, 1981.

5.   "Analysis of ECC Bypass Data," NUREG-0573, July, 1979.

6.   "Application of Battelle's Mechanistic Model to Lower Plenum
     Refill," NUREG/CR-2030, March, 1981.

7.   "Analysis of Flashing Transient Effects During Refill,"
     NUREG/CR-1765, March, 1981.

8.   "Summary of Refill Effects Studies with Flashing and ECC
     Interactions," NUREG/CR-2058, November, 1981.

9.   Weiss, P. A. and Hertlein, R. J.; "UPTF Test Results - First 3
     Separate Effects Tests," presented at the 14th Water Reactor Safety
     Information Meeting, October 27 - 31, 1986.

10. Richter, Horst J.; Wallis, Graham B; Carter, Kelly H. and
     Murphy, Stephen L.; "Deentrainment and Countercurrent Air-water Flow
     in Model PWR Hot Leg," Thayer School of Engineering, September, 1978

11. Gardner, G. C., "Flooded Countercurrent Two-phase Flow in Horizontal
     Tubes and Channels," Int. J. Multiphase Flow, Vol. 9, No. 4, 1983,
     pp. 367 through 382.

12. Wallis, G. B., "Flooding in Stratified Gas-liquid Flow," Dartmouth
     College Report No. 27327-9, August, 1970.

13. Ohnuki, A., "Experimental Study of Countercurrent Two-phase Flow in Horizontal Tube Connected to Inclined Riser," *Journal of Nuclear Science and Technology*, March, 1986, pp. 219 through 232.

14. Krolewski, S. M., "Flooding Limits in a Simulated Nuclear reactor Hot Leg," Massachusetts Institute of Technology, Submission as Part of Requirement for a B.Sc. (1980).

15. "Experiment Data Report for Semiscale Mod-2A Natural Circulation Tests S-NC-2B, S-NC-3, and SNC-4B," NUREG/CR-2454, prepared by EG&G Idaho, December 1981.

16. "Experiment Data Report for Semiscale Mod-2A Natural Circulation Tests S-NC-5 and S-NC-6," NUREG/CR-2501, prepared by EG&G Idaho, January 1982.

17. "PWR FLECHT-SEASET Systems Effects, Natural Circulation and Reflux Condensation," NUREG/CR-3654, EPRI NP-3497, WCAP-10415, prepared by Westinghouse Electric Corporation, August 1984.

18. Mandl, R. M., and Weiss, P. A., "PKL Tests on Energy Transfer Mechanisms during Small-break LOCAs," *Nuclear Safety*, Vol. 23, No. 2, March-April 1982.

19. Thompson, S. L., Kmetyk, L. N., "RELAP5 Assessment: PKL Natural Circulation Tests," prepared by Sandia National Laboratories, NUREG/CR-3100, SAND82-2902, January 1983.

20. Tasaka, K., et. al., "The Results of 5% Small-Break LOCA Tests and Natural Circulation tests at the ROSA-IV LSTF," presented at the Fourteenth Water Reactor Safety Information Meeting, October 27-31, 1986, NUREG/CP-0082, Volume 4.

Enclosure 2

Verification Analyses for Void Fraction Prediction